UNIVERSITY OF TARTU

FACULTY OF SCIENCE AND TECHNOLOGY

Institute of Chemistry

Ove Oll

In situ INFRARED SPECTROELECTROCHEMICAL MEASUREMENTS OF CARBON ELECTRODES IN IONIC LIQUID MEDIUM

Master's Thesis

Supervisor: PhD Tavo Romann

Accepted for commencement.....

Supervisor .....

signature, date

Tartu 2014

Table of Contents

1. Introduction 3

2. Literature overview 4

2.1. *In situ* spectroelectrochemistry 4

2.1.1. Infrared spectroelectrochemistry 4

2.1.2. *In situ* electroreflectance spectroscopy 5

2.2. Ionic liquids 6

2.1.1. 1-Ethyl-3-methylimidazolium tetrafluoroborate ($EMImBF_4$) 6

2.3. Electrochemistry 7

2.2.1. Electrical double layer 7

2.2.2. Electrochemistry of ionic liquids 8

3. Experimental 9

3.1. Equipment 9

3.2. Preparation of the electrodes 9

3.3. Infrared set-up 10

4. Results and analysis 11

4.1. Materials characterization 11

4.2. Electrochemistry 11

4.3. *In situ* infrared spectroscopy 13

4.4. Electrical double layer 16

4.5. Electrochemical breakdown 18

5. Summary 21

Kokkuvõte 22

7. References 23

8. Figures 28

9. Publications 44

1. Introduction

The processes taking place at carbon | electrolyte interfaces are of significant scientific importance due to their large role in the development of novel energy storage and conversion devices, including lithium and sodium ion batteries [1,2], pseudo- and supercapacitors [3,4] and fuel cells [5,6]. However, the vast majority of the research conducted in the field is focused on the materials science based understanding of materials and interfaces, while an understating based on fundamental electrochemistry is largely being ignored.

Ionic liquids are a novel type of solvent and electrolyte [7,8] with some unique properties compared to that of conventional aqueous or organic solvent based electrolytes, such as negligible vapor pressure, extremely wide electrochemical window and chemical inertness [9]. They also offer a multitude of opportunities as "designer" solvents due to the almost unlimited number of combinations of cations and anions they compose of and properties they have to offer [10]. While ionic liquids have been in the center of scientific interest for almost 15 years to date, the processes taking place at the interfaces of ionic liquids are still not very well understood [11]. On the contrary, a large amount of contradicting experimental and theoretical information exists on these topics. It is thus one of the main concerns of this thesis to try and provide an enhanced understanding of the interfacial properties of carbon | ionic liquid interfaces based on *in situ* infrared spectroscopy.

In situ infrared spectroscopy is an analytical method developed in the early 1970's [12] in order to provide a better understanding of both the structural and kinetic effects at metal | electrolyte interfaces. Although the literature concerning the use of metal electrodes for *in situ* infrared spectroelectrochemistry is vast [13], the use of pure carbon electrodes has largely been ignored. This thesis is an attempt to bridge that gap in scientific knowledge by measuring *in situ* infrared spectra for three different kinds of pure carbon electrodes with varied physical and chemical properties in order to provide a baseline for future studies of carbon interfaces by infrared spectroscopy.

The major purpose of this thesis is to combine classical electrochemistry measurements with novel *in situ* infrared spectroelectrochemical experiments in order to derive a better understanding of carbon | ionic liquid interfaces based on the models of fundamental electrochemistry.

2. Literature overview

2.1. *In situ* spectroelectrochemistry

The first studies of electrochemical phenomena with *in situ* spectroscopic techniques were conducted in the mid 60's [14] in order to "see" the processes taking place at the electrode surface. Since the ability to gain a quantifiable picture of the interfacial phenomena taking place at the surface of a working electrochemical system was of high value in a world where most interpretations and qualitative understanding of interfacial phenomena were based on the methods of "blind" electrochemistry, this spurred a great deal of interest in the development of these novel methods, with ultraviolet- visual (UV-Vis) and infrared spectroscopy being the first two types of spectroscopy to be applied for such studies. It should be noted, though, that while *in situ* spectroelectrochemical methods are commonplace today, most of these studies are focused on the reactions taking place at an electrode surface, studies of the electrical double layer [15,16] are much less prevalent due to the higher demands in terms of specificity and sensitivity of method and purity of the materials.

2.1.1. Infrared spectroelectrochemistry

The vibrational and rotational structure of a material is probed by infrared spectroscopy. This makes *in situ* infrared spectroscopic methods extremely valuable for the studies of interfacial phenomena, since both effects of structural change as well as that of interfacial concentration can be probed with high sensitivity. As the energy of the radiation associated with infrared spectroscopy is relatively low, these methods do not themselves cause adverse effects that could complicate the interpretation of spectra. That said, since the optics applied for *in situ* infrared spectroelectrochemistry are relatively complicated, the interpretation of these spectra is not always as clear and concise as one would like. As already mentioned, the primary focus of spectroelectrochemical studies with infrared radiation is on that of both single crystal and rough metallic electrodes, mostly because of the methods with enhanced sensitivity that have been developed for these materials. Because of the metallic properties of these materials, incident light polarized in the plane parallel to the surface has a much greater optical sensitivity of the adsorbate than that polarized in the direction normal to the surface [17]. Rough or roughened metallic surfaces also possess high surface plasmon activity and are thus suitable for interfacial studies incorporating plasmonic resonance [18]. In general, it is still unknown whether carbon electrodes possess similar properties or not, but the general

consensus and understanding [19] is that they do not, which is a major reason for why pure carbon electrodes have not been applied to many infrared spectroelectrochemical studies.

Two primary methods of *in situ* infrared spectroelectrochemistry are applied in this thesis: infrared absorption spectroscopy (IRAS) [20] and infrared reflection-absorption spectroscopy (IRRAS) [21]. Both have been applied in the attuned total-reflection (ATR) Kretschmann configuration [22]. These methods can be distinguished between by the optics at the interface of the electrodes- while in the IRAS method the interface is being probed by the evanescent wave caused by the reflection of light at the surface of an optical hemisphere, the IRRAS method primarily probes the radiation reflected at the working electrode surface. Both methods have their own strengths and weaknesses, but the application of one method or another is primarily based on the electrode material under study: only thin film electrodes can be used for the IRAS method while macroscopic electrodes are applicable for the IRRAS method. The technique of subtractively normalized interfacial Fourier transform infrared spectroscopy (SNIFTIRS) [23] is applied trough the thesis for the potential modulation in order to achieve interfacial sensitivity. The method applies the static measurement of spectra at a probed potential relative to that of an arbitrary reference potential as the background. Typically, the potential of zero charge (pzc) is chosen as the background potential for studies of the electrical double layer in order to simplify the interpretation of the spectra.

2.1.2. *In situ* electroreflectance spectroscopy

Electroreflectance (ER) spectroscopy is a widely used technique for the study of semiconductor electronic structure [24]. In the mid 60's it was discovered that the technique could also be used to probe metallic interfaces in *in situ* electrochemical conditions [25] using the external reflection technique with near infrared to ultraviolet irradiation. The thorough research that continued found that, differently from semiconductors, ER could be used to selectively probe the surface states of a metallic interface, thus providing an extremely powerful tool for the analysis of interfacial phenomena from an electronic standpoint. Although ER provided some fascinating insight into the electronic effects of metallic interfaces, many of the discovered experimental phenomena are still not adequately explained. Due to some technical difficulties and the fact that very few groups around the world had the knowledge and capability for *in situ* ER, the method was abandoned in the early 90's. *In situ* ER spectroscopy has not yet been applied for the study of carbon electrodes.

2.2. Ionic liquids

Ionic liquids are molten salts, although typically the term is only considered for materials with a melting point under 100 °C [7,8]. Another term, room-temperature ionic liquids is used for the characterization of salts with a melting point under 20 °C. Ionic liquids are slated to be composed of anions and cations only, which is largely responsible for their unique properties as both solvents and electrolytes. Ionic liquids and room-temperature ionic liquids are typically composed of large, asymmetric organic cations and highly coordinated symmetric anions [26]. Because of this general structure, the formation of a highly stable crystal lattice is inhibited, which is responsible for their relatively low melting point. Because of the ionic structure, ionic liquids also possess extremely low vapor pressure, which allows them to be used in ultra high vacuum (UHV) environments and to be purified in such environments. Studies have found that the vapor associated with ionic liquids is composed of ionic clusters [27], which is responsible for this abnormally low vapor pressure. Ionic liquids are generally chemically, electrochemically and thermally (up to 200-300 °C) stable [28,29], although many of the anions have a tendency to hydrolyze in the presence of water impurities [30,31]. Impurities are also one of the greatest concerns associated with ionic liquids as they tend to be difficult to purify post synthesis. Because a large number of ionic liquids are also hydrophilic, they tend to have a moderate concentration of water in them, even if only kept in the cleanest of environments. The major impurities associated with ionic liquids are water, halide and alkali ions and synthesis intermediates. Most ionic liquids have moderate to low [9] electrical conductivity, primarily caused by their relatively high viscosity.

2.1.1. 1-Ethyl-3-methylimidazolium tetrafluoroborate ($EMImBF_4$)

$EMImBF_4$ is one of the most often used ionic liquids for fundamental electrochemical studies [32–34]. The calculated gas phase ionic pair structure of $EMImBF_4$ is shown in Fig. 1. Because it is composed of relatively small ions, the use of $EMImBF_4$ in microporous carbon materials has been seen to offer slightly enhanced capacitance compared to that of more bulky ionic liquids [35], associated with a higher effective electrochemically active surface area. $EMImBF_4$ is also among the highest in electrical conductivity among ionic liquids [11] with a viscosity significantly lower than that of bulky pyrrolidinium based ionic liquids. It is also very well suited for infrared studies since it has strong and easily distinguishable absorption bands associated with both cations and anions. Those bands have also been seen to depend upon the interaction with one-another as well as that of the general chemical environment [36]. Among the negative qualities, $EMImBF_4$ has a relatively high melting point of 15 °C

[11] which significantly limits its use in systems of practical importance. The BF_4^- is also highly susceptible to hydrolysis in the presence of water impurities that can be caused by the relatively high hydrophilicity of the material. However, a major consideration of why the particular ionic liquid was chosen to study in this thesis is the commercial availability of highly pure forms of this material, which isn't the case for most ionic liquids.

2.3. Electrochemistry

Electrochemistry is the scientific discipline concerned with electronic and chemical structure of interfaces as well as their relation to electron transfer reactions. It is a highly branched discipline that interacts closely with materials science, colloidal science and interfacial physics as well as many other chemical sciences. In this thesis, two widely used methods of electrochemical analysis are applied in order to support the data measured by the spectroscopic methods. Cyclic voltammetry (CV) is applied in order to probe the width of electrochemical windows of the systems under study and to confirm that no residual faradic reactions take place at the electrode surface. Electrochemical impedance spectroscopy (EIS) is applied in order to rationalize the physical processes taking place at the interface as well as to measure the differential capacitance- potential (CE) curves for the systems under study. This data is correlated with the insights gained from spectroscopic measurements in order to make assessments about the electrical double layer structure formed at the interfaces of the systems under study.

2.2.1. Electrical double layer

The formation of an electrical double layer is based on the Volta problem [37,38], i.e. the differences in inner electric potential between two materials constituting an interface. This potential difference is screened at the interface by the effective charge carriers, polarizability and the orientational and spatial structure of the materials. Although modification of the dielectric electrolyte structure at a metal | electrolyte interface is by far the most studied part of the electrical double layer, in order to describe important properties of an interface, such as electrochemical activity or specific adsorption, one also has to consider the part of the electrical double layer inside an electrode material. While this is of little significance for the characterization of differential capacitance- potential curves for metal interfaces, the CE curves of both semiconductor and semimetal electrodes are largely dominated by this contribution, stemming from the formation of a space-charge layer [39] inside the electrode. It should also be noted that for materials for which the electronic structure can be described as

that of a two-dimensional electronic gas possess a different form of space-charge capacitance, one that is primarily limited by the density of electronic states of the material, called quantum capacitance [40]. Thus it has been shown that while the CE curves of highly oriented pyrolytic graphite (HOPG) can be described by the model of a semimetallic space-charge layer [39,41,42] and some contributions of quantum capacitance [40], the CE curves of graphene and few-layer graphene are primarily effected by the contributions from quantum capacitance [43].

While historic models of the electrical double layer, such as the Helmholtz [44], Gouy-Chapman [45] and Stern [46] models, focus exclusively on the electrostatic contributions to the screening of electronic charge, more recent considerations [38,47–49] have also emphasized the importance of dipole moments, dipole interactions, polarizability and compressibility of the electrolyte materials.

2.2.2. Electrochemistry of ionic liquids

As mentioned earlier, ionic liquids are advantageous for the use as electrolytes for electrochemical systems because of their high chemical and electrochemical stability [11]. Indeed, while supercapacitors applying aqueous or acetonitrile based electrolytes are limited to an electrochemical window of 2 or 2.8 V [3,50,51], supercapacitors based on ionic liquids have been applied to up to 3.5 V cell potentials [3]. That increase in cell potential does come at a price, though, as the high viscosity and low electrical conductivity mean that the power characteristics of such supercapacitors is not as high as those of electrolyte solutions [3]. The wide electrochemical window also means that ionic liquids can be used as a reaction medium for electrochemical synthesis and deposition, for which conventional electrolytes are ill suited for [8,9,52]. That said, the electrochemical properties of ionic liquids and the electrical double layer structure associated with them is still under intense study. Much of the early literature of these subjects is littered with studies where the purity of the materials had not been emphasized enough [11], and thus there is a great deal of contrasting information that has been published, because of which one should thread carefully when making assumptions about the electrochemistry of ionic liquids based on those earlier studies.

3. Experimental

3.1. Equipment

Amorphous carbon (aC) was deposited using AJA International Ultra high vacuum (UHV) magnetron sputtering system applying the following parameters: base vacuum 10^{-9} Torr, 3 mTorr Ar pressure, 200 W pulsed DC source (100 kHz, 3 msek), 50 W bias at the sample, sample temperature 190 °C, 3" graphite (99.999%) target. The film deposition rate 0.2 Å s^{-1} was controlled by using a quartz crystal microbalance. Atomic force microscopy (AFM) data were obtained by Agilent TechnologiesTM Series 5500 system. Raman spectra were taken with Renishaw inVia microRaman, using 514 nm laser exitation line. The infrared spectroscopic measurements were performed using a PerkinElmer Spectrum GX FTIR equipped with a liquid nitrogen cooled mid-range MCT detector and the electrochemical measurements were conducted using an Autolab PGSTAT 30 potentiostat in a three-electrode glass cell (Fig. 2) with an Ag|AgCl wire in the same IL for a pseudo-reference electrode (−0.156 V vs. ferrocene/ferrocenium couple [53]). Impedance spectra were measured within ac frequency range from 10^{-3} to 10^{5} Hz with 5 mV ac modulation. An ATR spectrum of $EMImBF_4$ liquid was measured separately using a Si hemisphere. $EMImBF_4$ from Solvionic (99.5 %, H2O ~100 ppm) was additionally dried in UHV at 100 °C for 48 h, until reaching a pressure of 10^{-9} Torr and water content below the detection limit of Karl Fischer method (<10 ppm).

3.2. Preparation of the electrodes

Magnetron sputtering of carbon is as simple as sputtering of gold, but the key aspect is the low conductivity of the thin carbon films prepared under normal sputtering conditions. Thus the sputtering parameters for the deposition of thin carbon films were optimized in this work. It was observed that the 20 nm thick carbon films directly sputtered onto the flat side of ZnSe hemisphere are suitable for *in situ* infrared absorption spectroscopy (IRAS) measurements (Fig. 3a).

A thin (~5 μm) HOPG layer is glued onto the ZnSe hemisphere with a thin layer (~300 nm) of dielectric epoxy (EPO) glue and exfoliated with scotch tape (Fig. 3a). Usually only one exfoliation is required to produce a see-trough layer of few-layer graphene (FLG) on the hemisphere. Although the produced surface is somewhat uneven, the hemisphere setup requires only the middle, infrared active part of the hemisphere to be uniformly covered.

Optical transmission and Raman spectroscopy measurements suggest the thinner parts of the electrode to compose of <10 layers of graphene.

The carbide-derived carbon (CDC) porous supercapacitor electrodes were prepared from 0.2-2 micrometer sized carbon powder (made from TiC by chlorination process [54]) + 5 % PTFE binder, roll-pressed to form a 100 μm thick electrode and sputter-coated with 2 μm thick Al layer in order to increase electronic conductivity. Aluminium contact layer is stable in dry $EMImBF_4$ due to the low solubility of formed Al_2O_3 and AlF_3 layers, but it should be noted that in the presence of 0.1 % water content Al would dissolve quickly. The specific surface area for microporous carbon SBET = 1860 $m^2\ g^{-1}$ was estimated according to the Brunauer–Emmett–Teller (BET) theory [55].

The infrared reflection-absorption spectroscopy (IRRAS) measurements applied 3 mm diameter CDC (Al layer facing upwards) electrodes pressed against an ATR hemisphere using perforated aluminium foil as a string and an electrical contact (Fig. 3b). IL immerses between the ZnSe and the electrode from the sides as the glass cell has 6 mm inner diameter.

3.3. Infrared set-up

Our constructed experimental system [56,57] uses 10 mm diameter infrared transparent ZnSe (infrared refractive index n = 2.4) hemisphere as the base for the working electrode (Fig. 2). The small glass cell also includes a Pt spiral counter electrode and a Luggin capillary for the connection of the reference electrode to the cell. 0.4 cm^3 $EMImBF_4$ was added into the dried cell inside an argon filled glove box, and the cell was thereafter sealed with PTFE stoppers. An IR beam was directed through a ZnSe wire grid polarizer (Pike Technologies) and a ZnSe lens to the ATR hemisphere at 65 degrees of incidence. IR measurements were carried out in an inert atmosphere at the temperature of 23 °C.

The spectra for positive and negative potentials were measured in separate experiments, starting from the potential of zero charge (pzc). 128 scans at a resolution of 4 cm^{-1} were collected at each potential and the measurement cycle was repeated 3 times. The resulting spectra were calculated by dividing the sample with the reference spectrum and presented as absorbance ΔA so that the positive-going bands represent a gain of a particular species at the sample potential relative to that at the reference potential. The measured bands were assigned to certain vibrations with the help of DFT-B3LYP/6-311+G** calculations applying GAUSSIAN 09 software. Calculated IR band frequencies were multiplied by 0.97, which is a common practice as the DFT calculation tends to overestimate the peak wavenumbers.

4. Results and analysis

4.1. Materials characterization

Fig. 4 shows the AFM topography images of both aC (a) and FLG (b) electrodes. It can be seen that the surface of the aC electrode is very flat, however, that the surface consists of small micro- and polycrystalline areas, as one would expect for an amorphous material. The surface of the FLG electrodes isn't quite as flat as that of aC electrodes, which is mostly due to the choice of substrate and thus the slightly wavy structure of the EPO glue is seen on the AFM image. That considered, the terraces on the electrode are seen to be of single layer height and there are large single crystal areas of C (0001) seen for the FLG electrode. The average width of the terraces for the FLG electrodes is over 4 μm. The CDC(TiC) electrodes used in this study have been previously characterized by electron microscopy, which show the electrodes as that of connected microcrystalline particles.

Raman spectra of the three different carbon electrodes are shown in Fig. 5. The spectrum of FLG is represented as that of HOPG due to the effect of substrate on the spectra. It can be seen that HOPG has only a single, very sharp peak representative of the G band vibration, which shows excellent quality of the material. Meanwhile, both the G band peak at 1587 cm^{-1}, representative of sp2 bonded microcrystalline areas as well as the D band peak at 1337 cm^{-1}, representative of disordered sp3 bonded areas, are seen for the CDC(TiC) electrode. These peaks are also significantly wider than that seen for HOPG, caused by the disorder in the structure of the material. The Raman peaks of aC are even wider as one would expect for a material with an amorphous structure. Only a single peak is seen at 1533 cm^{-1}, however it is clearly evident that the G and D bands are merged.

4.2. Electrochemistry

The CV graphs of the three different carbon materials measured in the $EMImBF_4$ ionic liquid are shown in Fig. 6. It can be seen that all three carbon materials afford a very wide electrochemical window in the ionic liquid. The cathodic and anodic limits of the electrochemical window for aC are slightly higher than that for the CDC and HOPG electrodes. Irreversible faradic current for the aC|$EMImBF_4$ system starts at ±2.05 V vs. Ag|AgCl, for an electrochemical window of 4.1 V. The electrochemical window for the HOPG electrode is somewhat narrower, from −1.9 V to +1.85 V for a total of 3.75 V. However, it can be seen that the cathodic breakdown for the HOPG electrode is somewhat reversible. This effect is interpreted to stem from the intercalation and subsequent

graphenisation effect caused by the intercalation of imidazolium cations into the graphite matrix, proven by the splitting of the G band peak in *ex situ* Raman measurements (not shown). As one would expect, the CV of the CDC electrode is largely different from that of aC and HOPG electrodes due to the extremely high specific surface area. The charging and discharging current dominates the voltammogram for the whole electrochemical window, which is again slightly narrower than that of aC, from −1.9 V to +1.6 V for a total 3.5 V, in agreement with what has been shown by 2-electrode measurements of the same material in the $EMImBF_4$ ionic liquid [58].

Electrochemical impedance spectroscopy phase angle diagrams measured at the pzc are shown in Fig. 7. The minimum phase angle for the HOPG|$EMImBF_4$ interface is seen to be −89.8 degrees, confirming the ideal polarizability of the system. The phase angle is seen to deviate from this value only slightly in a very wide frequency range, showing the lack of significant trace faradic reactions at the interface and excellent purity of both electrode and electrolyte materials. Meanwhile, due to the higher resistance associated with the aC electrode, the phase angle diagram is shifted to half a decade lower frequencies compared to that for HOPG. This higher resistance as well as non−uniformity of the electrode can also be associated with the higher phase angle values for the aC|$EMImBF_4$ interface. Again, the results for the CDC electrode differ widely from that of the flat electrodes. Because of the high diffusion resistance associated with diffusion of ions into the microporous structure of the CDC, the phase angle values are shifted over 4 orders of magnitude compared to that of the HOPG electrode. It is seen, however, that the formation of a plateau starts at extremely low frequencies (<10 mHz), associated with double layer capacitance of the electrode.

The differential capacitance- potential (CE) graphs for the three systems under study are shown in Fig. 8. The CE curve for the HOPG|$EMImBF_4$ system is typical of that of HOPG in other electrolytes with extremely low capacitance at the minimum and a general V-shape [39], mainly caused by the semimetallic nature of the C (0001) plane. The capacitance minimum at −0.2 V is also interpreted as the pzc of this system. Surprisingly, the aC|$EMImBF_4$ system shows a completely different CE curve with a high degree of hysteresis associated with the measurements starting at either anodic or cathodic potentials. Because of a low degree of graphitization for the aC electrodes, the electrodes can be considered as that of semiconductors with a moderate degree of free charge carriers associated with the defects in the carbon structure. Thus it is highly probable that the electric double layer extends through the entire 20 nm thickness of the electrode and that the hysteresis of the CE measurements can be associated with surface doping of ions, i.e. that of ion specific adsorption at surface defect

sites. Within such a consideration, the initial decrease of capacitance, measuring from either the cathodic or anodic side is due to desorption of ions at the surface, while the increase can be interpreted to be caused by the adsorption of counterions at the surface. The general magnitude of capacitance for both the HOPG and aC electrodes is approximately the same (~5 μF cm^{-2}) and the interpretation of pzc for the aC|$EMImBF_4$ interface is made based on the open-circuit potential at 0 V.

Because of the porous nature of the CDC electrode the capacitance is much higher than that of the flat electrodes. However, the general shape of the CE curve is very much similar to that of the HOPG electrodes. Interestingly, the minimum of capacitance for the CDC electrode is shifted by 0.4 V compared to that of the HOPG electrode, to 0.2 V. As is the case with HOPG electrodes, this minimum can be associated with the semimetallic nature of the material, while quantum capacitance [40] is also expected to play a large role in the formation of this minimum, which is interpreted to be the pzc. The shift in pzc for the materials is interpreted to stem from the difference in work function, i.e. the higher degree of dopants in the CDC structure compared to that of pristine HOPG. That considered, specific adsorption of ions at disordered parts of the CDC electrode can also play a role in this shift [57].

4.3. *In situ* infrared spectroscopy

The comparison between the ATR spectrum of $EMImBF_4$ calculated for monolayer adsorption [57] and the *in situ* IRAS spectrum of the aC|$EMImBF_4$ system at −1.6 V relative to 0 V is shown in Fig. 9. The interpretation of the major vibrations in the ATR spectrum of $EMImBF_4$ is given in Table 1.

Table 1: $EMImBF_4$ ATR spectrum interpretation.

Wavenumber / cm^{-1}	**Vibration type**	**Vibration characterization**
3164	ν	Symmetric H1; H2; H3 stretching
3124	ν	Asymmetric H1; H2; H3 stretching
1573	ν	Asymmetric C1; N1 stretching
1171	δ	H1 in-plane rocking
1037	ν	B-F stretching
848	δ	H1 out-of-plane rocking
756	δ	H2; H3 out-of-plane rocking
704	δ	H1; H3 out-of-plane twisting

ν – valence band, δ – deformation band

It can be seen that the *in situ* spectrum is weaker than that of the ATR spectrum calculated for monolayer adsorption, which confirms the earlier assumptions about the lack of an enhancement effect associated with the aC electrode. The peaks for the *in situ* spectrum represent about 60% of the intensity of the monolayer absorbance and the peaks for cations and anions follow a general trend expected for dense double layer formation via direct charge compensation of electrode surface charge density. It can also be seen that the absorption peaks are at lower wavenumbers compared to that of the ATR spectrum. This in general confirms the earlier assumptions made about the aC|EMImBF$_4$ interface based on the CE curve that the change in capacitance is largely defined by the specific adsorption of ions.

The potential dependence of the IRAS spectra of the aC|EMImBF$_4$ interface are shown in Fig. 10. The same general trends described previously can also be seen for the whole width of the electrochemical window- an increase of cation (1166 cm^{-1}) and decrease of anion (1020 cm^{-1}) surface concentration at cathodic potentials and vice versa.

The potential dependence of the *in situ* IRRAS spectra of the CDC(TiC)|EMImBF$_4$ system are shown in Fig. 11. The spectra are very different from that of the aC interface. Firstly, they are a lot more intensive, as one would expect for a material with a higher specific surface area. However, it is seen that all the peaks in the spectra, both at cathodic and anodic potentials, are in the same direction and negative relative to the reference potential. It should also be noted that there are no significant changes in the adsorption values of the major peaks in the spectra, compared to that of the ATR spectrum and the relative peak areas for the major anion and cation peaks matches that for the ATR spectrum, at approximately 15-to-1. It should be noted that because of symmetry considerations, the BF_4^- anion in gas phase does not actually possess an infrared active B−F symmetric stretching vibration and thus the intensity of this peak is defined by the interaction between cations and anions in the ionic liquid structure. Thus it is concluded, similar to a recent *in situ* infrared study about a compareable interface [59] that these peaks do not represent changes at the interface of the CDC electrode and instead stem from the changes in the thin ionic liquid layer between the ZnSe hemisphere and the CDC electrode. It is seen that because of the actuation of the porous carbon matrix, ionic liquid absorbed by the electrode decreases the amount of ionic liquid in the thin layer, which is detected by our measurements. No significant effect of charge separation is seen based on these results, hinting at a high degree of dipole polarization at the interface. Similar results have also been produced for CDC electrodes with *in situ* quartz crystal microbalance [60] and dilatometry [61,62] methods.

The p-polarized *in situ* IRAS spectra of the FLG|EMImBF$_4$ interface are shown in Fig. 12 and Fig. 13. It should be noted that, similar to what was found for thin-film bismuth electrodes [56], the s-polarized spectra are more intensive and show the opposite potential dependence compared to the p-polarized spectra, which can be explained by the semimetallic nature of the materials. This means that if one were to measure potential dependent *in situ* IRAS spectra with FLG without polarized light, the spectra would not be representative of the changes at the interface. It is seen that, again, the produced spectra are very different from those of both the aC interface and the CDC interface. Firstly, there are spectral features present that are not commonly seen for thin film measurements of *in situ* infrared spectra. Extremely wide (approximately 1000 cm^{-1} wide) Gaussian shaped peaks with a strong dependence on the electrode potential are detected. These peaks are interpreted to stem from the electroreflectance effect, commonly seen in the UV-Vis spectra of metal interfaces [63]. Strong peaks representative of the G-band vibration of the FLG electrode are also seen. These features will be discussed in more detail later. Similar to the spectra produced for the CDC electrode, the IRAS spectra for the FLG|EMImBF$_4$ interface are extremely intensive, while the major cation and anion vibrations are seen to be pointing in the same direction, regardless of applied potential. However, different from that of the CDC|EMImBF$_4$ interface, these peaks all show a gain of the relative species in relation to the pzc and thus match the general logic of the CE curve. Also, the peak for the anion vibration is shifted significantly compared to the ATR spectrum to 1020 cm^{-1}, similar to that seen at the aC interface. It should also be noted that the peak area ratio between the major anion (1020 cm^{-1}) and cation (1171 cm^{-1}) vibrations is seen to be significantly different from that of the ATR spectrum, at 22-to-1 ratio, compared to a 15-to-1 ratio seen for both the ATR spectrum and the CDC|EMImBF$_4$ interface, which is indicative of a major change in the interaction between cation and anion species in the probed region. All these effects suggest that these peaks are indeed representative of the electrical double layer. However, it seems illogical that the spectra for the FLG|EMImBF$_4$ interface are about 50 times as intensive as those seen for the aC|EMImBF$_4$ interface, when both are measured in the same principal thin film configuration. Even accounting for the differences in electrical double layer structure and electrode thickness (<5 nm for FLG and 20 nm for aC), such increase of signal intensity is rare even for rough metallic surfaces and comparison with the monolayer ATR spectrum would lead one to believe that the electrical double layer is over 100 monolayers thick. Theoretical models [64] and experiments with graphene micro-ribbons [65] have predicted that the plasmonic resonance of graphene is applicable for spectroscopy in the terahertz frequency range. A

recent article [66] has also shown that graphene nano-ribbon arrays exhibit plasmonic enhancement of adsorbed structures. Thus, it is concluded that the plasmonic resonance of graphene [67] is indeed applicable for the investigation of the electrical double layer structure and is the source of this significant enhancement at the interface of FLG electrodes. The first article to show this effect for graphene nanoribbons [66] also demonstrated that the enhancement effect for graphene extends much deeper into the adsorbate structure compared to that of the conventional SEIRA effect for metal electrodes [16], which is considered to exclusively enhance the spectral features of only the contact layer of the electrode. The enhancement for graphene, however, is seen to extend atleast 8 nm from the interface and is thus very well suited to study the changes in the diffuse part of the electrical double layer.

4.4. Electrical double layer

Finally, we can discuss the implications of both the electrochemical measurements and the *in situ* infrared spectra on the electrical double layer structure associated with these electrodes. The integrated peak areas associated with both the major anion and cations vibrations are shown in Fig. 14 for the aC|$EMImBF_4$ interface, Fig. 15 for the CDC(TiC)|$EMImBF_4$ interface and Fig. 16 for the FLG|$EMImBF_4$ interface. As discussed previously, these results represent very different spectral dependences, dependent on both the electrical double layer structure and spectral logic.

The electrical double layer formation at the aC interface has already been discussed based on the properties of the material and the CE curves. Despite the high degree of spectral noise associated with these measurements, which is to be expected for unenhanced spectra of sub-monolayer changes, the linear trendlines of the spectral dependences represent well the previously proposed model of electrode surface doping of ions, as by far the most important form of screening seen for these electrodes is based on direct charge compensation in the dense layer.

As the CE curves of both the CDC and FLG electrodes both stem from the same physical phenomena and show an extremely similar general shape, one would assume that the electrical double layer structure associated with these materials would also be similar. However, as previously discussed and seen from Fig. 15 and 16, that is not the case- a slightly trounced parabolic potential dependence with a maximum near the pzc is seen for the CDC electrode while a general V-shaped potential dependence with a minimum at pzc is observed for the FLG interface. For both electrodes, little in terms of direct charge compensation is seen as both the cation and anion peaks follow the same general trends. Even considering the

previously proposed thin layer explanation for the CDC electrodes, one would expect that if direct charge compensation was the major mechanism of potential screening in the electrical double layer, the thin layer would also be enhanced with one ion more so than the other. It should be noted, though, that the models of the electrical double layer that consider direct charge compensation the only form of electrode charge screening, such as the Gouy-Chapman diffuse double layer theory , were proposed prior to the advent of the dipole moment Debye, or any of the interactions associated with dipole moments. That said, even as early as 1928 [38,47] the strong dipole moment of water was used to explain the large difference of pzc between Hg and Ga interfaces relative to that of their work functions. Many of the latter models of the electrical double layer have also emphasized the importance of dipole screening in the electrical double layer [38], though such models have not seen very wide acceptance among the scientific community, primarily due to their relative complexity. Another point of emphasis is that, even as early as 1972, it was shown [39] that the differential capacitance of HOPG in nonspecific aqueous electrolyte solutions has an extremely weak dependence on the electrolyte concentration in a very wide range of electrolyte concentrations, from 10^{-5} M to 0.9 M solutions. Based on this knowledge, the interpretation that HOPG acts in electrolyte solutions as a semimetal was made; however, those results also show that direct charge compensation in the the diffuse part of the electrical double layer can not be of major importance for these systems. This is also the conclusion this thesis arrives at based on the CE curves and the *in situ* infrared results- the screening of the electrical potential difference for graphite and graphene based materials is largely governed by the formation of a dipole lattice at the electrode surface. This lattice of weakly structured electrolyte at the electrode interface can screen either positive or negative surface charge densities based on the collective dipole of the structured layer. A similar consideration of the screening of potential difference can be seen for solid dielectrics in dielectric capacitors, where the electrical charge at the metal electrodes is screened by the induced polarizability of the dielectric and not charged species.

Now we come back to the electroreflectance and G band peaks observed for the FLG|EMImBF$_4$ interface shown in Fig. 17. It can be seen that both of these features represent the same basic V-shaped potential dependence as that seen for the CE curves of HOPG and CDC electrodes, as well as the anion and cation peak intensity seen in the same spectra, and it is highly unlikely to be so coincidentally. That said, all the previously named features stem from slightly different physical phenomena. Based on the theory of *in situ* ER spectroscopy, the wide adsorption bands in the *in situ* infrared spectra of the FLG|EMImBF$_4$ interface represent the empty surface electronic bands, to which electrons can be excited by infrared

radiation. Thus it is the surface electronic structure that is being probed by these features. The fact that the absolute slope (0.233 eV V^{-1}) at both the anode and cathode side is of the same value is representative of the fact that no specific adsorption occurs at the FLG surface and thus the empty electronic bands of the surface are not modified by the adsorbate structure. As discussed under Raman spectroscopic characterization of the carbon materials, the G band is representative of the sp2 carbon vibrations. Moreso, *in situ* Raman spectroscopic measurements of graphene [68] have shown this feature to be extremely sensitive to the electrode surface charge, which both the wavenumber and intensity of this vibration are dependent upon. The same principal effect is seen for our measurements, as the location of this peak strongly depends on the electrode potential. Based on this knowledge, one is lead to believe that, as is the case in electrolyte solutions [39], the shape of the CE curves of graphite and graphene based materials is largely defined by the electrode material [43]. A different viewpoint was expressed in a recent theoretical paper [69] attempting to explain the CE curves of ionic liquid interfaces with graphite in terms of the formation of two double layers. Based on the results shown in this thesis, however, those considerations can be seen as oversimplified and that more comprehensive models are required in order to explain the capacitance of ionic liquid interfaces. Indeed, considering both the electronic structure of graphene [70] and the *in situ* IRAS spectra shown for the FLG|$EMImBF_4$ interface, one is lead to believe that it is truly a case of one, complex double layer and not the addition of many arbitrary, noninteracting layers, as considered by the theoretical article [69] and historic electric double layer theories [38]. That said, this can not be either confirmed or denied at the present state of knowledge and extensive research would be required to do so.

4.5. Electrochemical breakdown

The IRAS spectrum of the aC|$EMImBF_4$ interface at −2.4 V, shown in Fig. 18, is quite different from the spectrum of $EMImBF_4$ liquid (Fig. 9) or IRAS spectra measured at more electrode positive potentials (Fig. 8). It can be seen that the negative-going peaks belong to $EMImBF_4$ (indication of desorption of ionic liquid from the surface) whereas the positive-going peaks (2971, 2943, 2872, 2848, 2814, 1608, 1445, 1371, 1345, 1244, 1141, and 724 cm^{-1}) are totally different from the $EMImBF_4$ spectrum, suggesting that a new compound has formed. The spectrum in Fig. 9 is in a good agreement with the calculated IR spectrum of 1,5-diethyl-4,8-dimethyl-1,4,5,8-tetraazafulvalene, indicating that at $E < -2$ V the EMIm+ cation decomposes to hydrogen and the dimer formation takes place (reaction scheme is given in Fig. 18b). Strong positive peaks indicate to the formation of a thick layer of the dimer.

A different dimer, with two hydrogens at C1 and C1' present, has also been proposed as a product [71], but the visible formation of hydrogen bubbles yields to the conclusion that the dimer in Fig. 18b is the compound that forms.

It has to be noted that for the CDC electrode, the spectra for the cathodic product was not detected even at −3.4 V (not shown), likely due to the production of H2 gas bubbles in the pores, which causes a significant ohmic drop.

The anodic oxidation reaction starts at +1.6 V for the CDC electrode, at +1.85 V for the HOPG electrode, and only at +2.05 V for the aC film. The double bonds in the graphene sheets of HOPG are more prone to react compared to somewhat more tetrahedral bonds at the surface of the aC electrode. The higher catalytic behavior of CDC electrode is due to the porous surface, which probably reduces the reaction activation energy.

Elemental fluorine evolution from solutions containing fluoride anions has a thermodynamic value of +2.87 V vs. NHE [72], which is about +2.6 V vs. our reference electrode. Therefore, the direct fluorine formation should not take place at $+1.6 < E < +2.4$ V, but some kind of fluorination reaction definitely occurs. According to cyclic voltammetry data in Fig. 5, the anodic process is totally irreversible, but fluorinated graphite has found use in batteries [73] and if a fluorocarbon forms, it should give some reduction peaks at more positive potentials.

There is a wide peak at 1224 cm^{-1} and extremely sharp peak at 835 cm^{-1} in the infrared spectra for all three carbons – indicative of the formation of new compounds, while the negative peaks belong to $EMImBF_4$ and indicate the desorption of IL from the electrode surface. A peak at 1200 cm^{-1} was measured in the IR spectra of graphite fluoride (with molecular composition C:F = 1:1, obtained from Sigma-Aldrich), shown in Fig. 19a. The fact that the IR spectra at E = 2 V are very similar for the three different carbons indicates rather the formation of some fluorinated product and not the C-F bond at the carbon surface. Ex situ measurements (after removal of $EMImBF_4$) did not give any IR peaks characteristic for carbon fluoride [74]. The trace anodic fluorination of carbon has been detected by the XPS method for glassy carbon [75], but not for HOPG and doped diamond electrodes [75] in the anhydrous solutions containing BF_4− anions. Therefore, it can be concluded that the IR peaks at 1224 cm^{-1} and 835 cm^{-1} are caused by the formation of some molecular products.

The formation of BF_3 has been proposed in Refs. [76] and [77], however, the experimental spectrum of BF_3 gas has IR peaks at 1453 and 693 cm^{-1}, which do not match with the measured *in situ* spectra. BF_3 is a strong acid and gives various compounds with organic molecules. Therefore, we have calculated several BF_3 complexes and some of these appear to have infrared peaks near 1230 cm^{-1} (Fig. 19a). Combination of BF_3 with BF_4^- anion gives a

stable product $B_2F_7^-$; the calculated IR spectra of $EMIm^+$ $B_2F_7^-$ ion-pair has asymmetric stretch peaks near 1167 cm^{-1}. Also, BF_3 complex with some fluorinated product may be considered as the source for the peak at 1224 cm^{-1}. The fluorination may occur at the side chains as such processes have been described in the literature - electrochemical fluorination of toluene results in methyl group fluorination [78]. Electrochemical fluorination can proceed as an addition to the double bond, replacement of a hydrogen atom or cleaving of the nitrogen-carbon bonds [78].

The sharp peak at 835 cm^{-1} is connected with the symmetric vibration of a tetrahedral $X+BF_3$ group. In the literature, there is an IR spectrum of BF_3-imidazolium product, where the BF_3 group is attached to the C2 position, but there is no sharp peak near 835 cm^{-1} [79]. However, the calculated spectra of the compound, where BF_3 is attached to the imidazolium N atom, gives a strong peak at 837 cm^{-1}, which indicates that the fluorination reaction might lead to the cleaving of N-C bond and formation of the imidazolium trifluoroborate derivatives is possible. Among the calculated theoretical products, the substance given in Fig. 19b (1-methyl-3-trifluoroboroimidazole - $MImBF_3$) has the lowest energy as well as the best fit with the experimentally measured spectra.

5. Summary

Cyclic voltammetry, electrochemical impedance spectroscopy as well as *in situ* infrared spectroscopy have been applied for the study of three different pure carbon materials in an ionic liquid electrolyte in order to gain a better understanding of the processes taking place at the interfaces of the materials. Physical characterization of the materials has been done by atomic force microscopy and Raman spectroscopy measurements, showing significant structural and electronic differences between the materials.

The electrochemical measurements showed that while the amorphous carbon (aC) electrode can best be described as a semiconductor, the differential capacitance- potential (CE) curves of the porous carbon derived carbon (CDC) and highly oriented pyrolitic graphite (HOPG) are rather similar, stemming from the semimetallic nature of graphite.

Two new electrodes have been applied for *in situ* infrared measurements, providing new opportunities for future studies of carbon interfaces. It has been shown that although porous CDC electrodes are generally not well suited for the study of the electrical double layer structure by infrared spectroscopy, the *in situ* infrared spectra of aC and FLG electrodes in ionic liquid medium are well suited for these kinds of studies. For the first time, the *in situ* electroreflectance (ER) and plasmonic enhancement effects have been shown for a pure carbon electrode.

Based on both the electrochemical and spectroscopic data, a general understanding of the electrical double layer formation at the three carbon electrodes has been provided. Both the CE curves and spectral data suggest that the differential capacitance of the aC electrodes is largely affected by specific ion interactions at the electrode surface and that direct charge compensation in the dense layer is primarily responsible for the capacitance behavior at the electrolyte side of the electrical double layer. Meanwhile, analysis of the spectral data for both the CDC and FLG electrodes is indicative of the fact that dipole interactions are of great importance for the screening of the electrical potential difference and surface charge at the interfaces of these materials. The importance of a comprehensive consideration of the formed electrical double layer is also emphasized based on the combined understanding of the IRAS, ER and CE data for the FLG|EMImBF_4 interface.

In situ infrapuna spektroelektrokeemia mõõtmised süsinikelekdroodidel ioonse vedeliku keskkonnas

Ove Oll

Kokkuvõte

Tsüklililise voltamperomeetria, elektrokeemilise impedantsi spektroskoopia ja *in situ* infrapunaspektroskoopia meetodeid kasutati kolme erineva süsinikelektroodi elektrokeemiliste omaduste iseloomustamiseks ioonse vedeliku keskkonnas, et omandada parem arusaam materjalide piirpindadel toimuvatest füüsikalistest protsessidest. Materjale iseloomustati lisaks ka aatomjõu mikroskoopia ja Raman spektroskoopia meetoditega.

Elektrokeemilised mõõtmised näitasid, et kui amorfne süsinik (aS) on pigem iseloomustatav kui pooljuht materjal, siis poorse karbiidse süsiniku (KS) ja kõrgorienteeritud pürolüütilise grafiidi (KOPG) differentsiaalmahtuvuse potentsiaalist sõltuvuse (ME) kõverad on üsnagi sarnased, mis tuleneb vastavate materjalide poolmetallilistest omadustest.

In situ infrapuna spektroelektrokeemia mõõtmisteks tutvustati kaht uut elektroodi materjali, mis loovad uusi võimalusi pindprotsesside uurimiseks vastavate elektroodide piirpindadel. Näidati, et kuigi KS ei ole hästi sobilik infrapunaspektroskoopiliseks elektrilise kaksikkihi iseloomustamiseks, siis nii mõnekihiline grafeen (MKG) kui aS pakuvad häid võimalusi vastavate uuringute teostamiseks ioonse vedeliku keskkonnas. Esmakordselt demonstreeriti *in situ* elektroneeldumise ja plasmonite resonantsi meetodeid puhtakujulistel süsinikelektroodidel.

Elektrokeemia ja spektroskoopia meetodite tulemuste põhjal loodi üldine arusaam uuritavate süsinikelektroodide piirpindadel toimuvatest protsessidest. Nii ME kõverad kui ka spektroskoopia andmed viitavad, et aS differentsiaalmahtuvus on suuresti mõjutatud ioonide spetsiifilisest interaktsioonist piirpinnaga, ning et mahtuvuslik käitumine elektrilise kaksikkihi elektrolüüdi osas antud süsteemis on peamiselt põhjustatud otsesest laengu kompensatsioonist elektrilise kaksikkihi tihedas osas. Samaaegselt viitab KS ja MKG spektrite analüüs, et dipool moment ja selle interaktsioonid on äärmiselt olulisel kohal vastavates süsteemides elektrilise potentsiaali erinevuse ja pinnalaengu ekraneerimisel. Samuti tähtsustatakse komplektset mõistmist elektrilise kaksikkihi struktuurist, mis tuleneb infrapuna adsorptisioonispektroskoopia, elektroneeldumise ja differentsiaalmahtuvuse andmetest MKG|1-etüül-3-metüülimidazoolium tetrafluoroboraadi süsteemi kohta.

7. References

[1] V. Etacheri, R. Marom, R. Elazari, G. Salitra, D. Aurbach, Challenges in the development of advanced Li-ion batteries: a review, Energy Environ. Sci. 4 (2011) 3243–3262.

[2] M. Ishikawa, M. Yamagata, T. Sugimoto, Y. Atsumi, T. Kitagawa, K. Azuma, Li-Ion Battery Performance with FSI-Based Ionic Liquid Electrolyte and Fluorinated Solvent-Based Electrolyte, ECS Trans. 33 (2011) 29–36.

[3] L. Zhang, F. Zhang, X. Yang, G. Long, Y. Wu, T. Zhang, et al., Porous 3D graphene-based bulk materials with exceptional high surface area and excellent conductivity for supercapacitors, Sci Rep. 3 (2013).

[4] T. Kim, H. Lee, J. Kim, K.S. Suh, Synthesis of Phase Transferable Graphene Sheets Using Ionic Liquid Polymers, Acs Nano. 4 (2010) 1612–1618.

[5] E. Antolini, Carbon supports for low-temperature fuel cell catalysts, Appl. Catal. B Environ. 88 (2009) 1–24.

[6] H. Chang, S.H. Joo, C. Pak, Synthesis and characterization of mesoporous carbon for fuel cell applications, J. Mater. Chem. 17 (2007) 3078–3088..

[7] T. Welton, Room-temperature ionic liquids. Solvents for synthesis and catalysis, Chem. Rev. 99 (1999) 2071–2084.

[8] M. Armand, F. Endres, D.R. MacFarlane, H. Ohno, B. Scrosati, Ionic-liquid materials for the electrochemical challenges of the future, Nat. Mater. 8 (2009) 621–629.

[9] H. Ohno, Electrochemical Aspects of Ionic Liquids, John Wiley & Sons, 2011.

[10] M.J. Earle, K.R. Seddon, Ionic liquids. Green solvents for the future, Pure Appl. Chem. 72 (2000) 1391–1398.

[11] M.V. Fedorov, A.A. Kornyshev, Ionic liquids at electrified interfaces, Chem. Rev. 114 (2014) 2978–3036.

[12] K. Ashley, S. Pons, Infrared spectroelectrochemistry, Chem. Rev. 88 (1988) 673–695.

[13] T. Iwasita, F.C. Nart, In situ infrared spectroscopy at electrochemical interfaces, Prog. Surf. Sci. 55 (1997) 271–340.

[14] T. Kuwana, R.K. Darlington, D.W. Leedy, Electrochemical Studies Using Conducting Glass Indicator Electrodes., Anal. Chem. 36 (1964) 2023–2025.

[15] M. Osawa, In-situ Surface-Enhanced Infrared Spectroscopy of the Electrode/Solution Interface, in: R.C. Alkire, D.M. Kolb, J. Lipkowski, P. Ross (Eds.), Adv. Electrochem. Sci. Eng., Wiley. com, 2006.

[16] M. Osawa, K. Ataka, K. Yoshii, T. Yotsuyanagi, Surface-enhanced infrared ATR spectroscopy for in situ studies of electrode/electrolyte interfaces, J. Electron Spectrosc. Relat. Phenom. 64–65 (1993) 371–379.

[17] M. Moskovits, Surface selection rules, J. Chem. Phys. 77 (1982) 4408–4416.

[18] M. Osawa, Dynamic processes in electrochemical reactions studied by surface-enhanced infrared absorption spectroscopy (SEIRAS), Bull. Chem. Soc. Jpn. 70 (1997) 2861–2880.

[19] A.J. Bard, M. Stratmann, P.R. Unwin, eds., Encyclopedia of Electrochemistry: Instrumentation and Electroanalytical Chemistry v. 3, Wiley VCH, 2003.

[20] Y.J. Chabal, K. Raghavachari, Applications of infrared absorption spectroscopy to the microelectronics industry, Surf. Sci. 502 (2002) 41–50.

[21] C.-M. Pradier, M. Salmain, Z. Liu, C. Methivier, Comparison of different procedures of biotin immobilization on gold for the molecular recognition of avidin: an FT-IRRAS study, Surf. Interface Anal. 34 (2002) 67–71.

[22] E. Kretschmann, H. Raether, Radiative decay of non radiative surface plasmons excited by light(Surface plasma waves excitation by light and decay into photons applied to nonradiative modes), Z. Fuer Naturforschung Teil A. 23 (1968) 2135.

[23] N.S. Marinković, M. Hecht, J.S. Loring, W.R. Fawcett, A sniftirs study of the diffuse double layer at single crystal platinum electrodes in acetonitrile, Electrochimica Acta. 41 (1996) 641–651.

[24] M. Cardona, K.L. Shaklee, F.H. Pollak, Electroreflectance at a semiconductor-electrolyte interface, Phys. Rev. 154 (1967) 696.

[25] J. Feinleib, Electroreflectance in Metals, Phys. Rev. Lett. 16 (1966) 1200.

[26] R.D. Rogers, Materials science - Reflections on ionic liquids, Nature. 447 (2007) 917–918.

[27] M.J. Earle, J.M.S.S. Esperança, M.A. Gilea, J.N.C. Lopes, L.P.N. Rebelo, J.W. Magee, et al., The distillation and volatility of ionic liquids, Nature. 439 (2006) 831–834.

[28] M. Kosmulski, J. Gustafsson, J.B. Rosenholm, Thermal stability of low temperature ionic liquids revisited, Thermochim. Acta. 412 (2004) 47–53.

[29] H.L. Ngo, K. LeCompte, L. Hargens, A.B. McEwen, Thermal properties of imidazolium ionic liquids, Thermochim. Acta. 357 (2000) 97–102.

[30] K.R. Seddon, A. Stark, M.-J. Torres, Influence of chloride, water, and organic solvents on the physical properties of ionic liquids, Pure Appl. Chem. 72 (2000) 2275–2287.

[31] K.N. Marsh, J.A. Boxall, R. Lichtenthaler, Room temperature ionic liquids and their mixtures - a review, Fluid Phase Equilibria. 219 (2004) 93–98.

[32] A. Lewandowski, M. Galiński, Carbon–ionic liquid double-layer capacitors, J. Phys. Chem. Solids. 65 (2004) 281–286.

[33] P. Diao, Z.F. Liu, Electrochemistry at chemically assembled single-wall carbon nanotube arrays, J. Phys. Chem. B. 109 (2005) 20906–20913.

[34] M.F. El-Kady, V. Strong, S. Dubin, R.B. Kaner, Laser scribing of high-performance and flexible graphene-based electrochemical capacitors, Science. 335 (2012) 1326–1330.

[35] L. Zhang, X. Yang, F. Zhang, G. Long, T. Zhang, K. Leng, et al., Controlling the Effective Surface Area and Pore Size Distribution of sp2 Carbon Materials and Their Impact on the Capacitance Performance of These Materials, J. Am. Chem. Soc. 135 (2013) 5921–5929.

[36] N.E. Heimer, R.E. Del Sesto, Z. Meng, J.S. Wilkes, W.R. Carper, Vibrational spectra of imidazolium tetrafluoroborate ionic liquids, J. Mol. Liq. 124 (2006) 84–95.

[37] A. Volta, Phil Mag. 7 (1800).

[38] B.B. Damaskin, O.A. Petrii, Historical development of theories of the electrochemical double layer, J. Solid State Electrochem. 15 (2011) 1317–1334.

[39] J.-P. Randin, E. Yeager, Differential capacitance study on the basal plane of stress-annealed pyrolytic graphite, J. Electroanal. Chem. Interfacial Electrochem. 36 (1972) 257–276.

[40] H. Gerischer, R. McIntyre, D. Scherson, W. Storck, Density of the electronic states of graphite: derivation from differential capacitance measurements, J. Phys. Chem. 91 (1987) 1930–1935.

[41] H. Gerischer, An interpretation of the double layer capacity of graphite electrodes in relation to the density of states at the Fermi level, J. Phys. Chem. 89 (1985) 4249–4251.

[42] H. Gerischer, The impact of semiconductors on the concepts of electrochemistry, Electrochimica Acta. 35 (1990) 1677–1699.

[43] H. Ji, X. Zhao, Z. Qiao, J. Jung, Y. Zhu, Y. Lu, et al., Capacitance of carbon-based electrical double-layer capacitors, Nat. Commun. 5 (2014).

[44] H. von Helmholtz, Ueber einige Gesetze der Vertheilung elektrischer Ströme in körperlichen Leitern mit Anwendung auf die thierisch-elektrischen Versuche, Ann. Phys. 165 (1853) 211–233.

[45] G.L. Gouy, J. de Phys., 9, 457; Chapman, DL, 1913, Lond. Edinburg Phil Mag J Sci. 25 (1910) 475.

[46] O. Stern, The theory of the electrolytic double-layer, Zeit Elektrochem. 30 (1924) 508–516.

[47] B.B. Damaskin, A.N. Frumkin, Potentials of zero charge, interaction of metals with water and adsorption of organic substances—III. The role of the water dipoles in the structure of the dense part of the electric double layer, Electrochimica Acta. 19 (1974) 173–176.

[48] D.C. Grahame, The electrical double layer and the theory of electrocapillarity., Chem. Rev. 41 (1947) 441–501.

[49] A.A. Kornyshev, Double-layer in ionic liquids: paradigm change?, J. Phys. Chem. B. 111 (2007) 5545–5557.

[50] Q.T. Qu, B. Wang, L.C. Yang, Y. Shi, S. Tian, Y.P. Wu, Study on electrochemical performance of activated carbon in aqueous Li2SO4, Na2SO4 and K2SO4 electrolytes, Electrochem. Commun. 10 (2008) 1652–1655.

[51] Q. Zhang, Y. Han, Y. Wang, S. Ye, T. Yan, Comparing the Differential Capacitance of two Ionic Liquid Electrolytes: Effects of Specific Adsorption, Electrochem. Commun. (n.d.).

[52] S. Zein El Abedin, K.S. Ryder, O. Höfft, H.K. Farag, Ionic Liquids: Potential Electrolytes for Electrochemical Applications, Int. J. Electrochem. 2012 (2012) 1–2.

[53] M.T. Alam, M. Mominul Islam, T. Okajima, T. Ohsaka, Measurements of differential capacitance in room temperature ionic liquid at mercury, glassy carbon and gold electrode interfaces, Electrochem. Commun. 9 (2007) 2370–2374.

[54] M. Arulepp, L. Permann, J. Leis, A. Perkson, K. Rumma, A. Jänes, et al., Influence of the solvent properties on the characteristics of a double layer capacitor, J. Power Sources. 133 (2004) 320–328.

[55] K. Tõnurist, T. Thomberg, A. Jänes, T. Romann, V. Sammelselg, E. Lust, Influence of separator properties on electrochemical performance of electrical double-layer capacitors, J. Electroanal. Chem. 689 (2013) 8–20.

[56] T. Romann, O. Oll, P. Pikma, E. Lust, Abnormal infrared effects on bismuth thin film–EMImBF4 ionic liquid interface, Electrochem. Commun. 23 (2012) 118–121.

[57] T. Romann, O. Oll, P. Pikma, H. Tamme, E. Lust, Surface chemistry of carbon electrodes in 1-ethyl-3-methylimidazolium tetrafluoroborate ionic liquid – an in situ infrared study, Electrochimica Acta. 125 (2014) 183–190.

[58] H. Kurig, A. Jänes, E. Lust, Electrochemical Characteristics of Carbide-Derived Carbon| 1-Ethyl-3-methylimidazolium Tetrafluoroborate Supercapacitor Cells, J. Electrochem. Soc. 157 (2010) A272–A279.

[59] F.W. Richey, B. Dyatkin, Y. Gogotsi, Y.A. Elabd, Ion Dynamics in Porous Carbon Electrodes in Supercapacitors Using in Situ Infrared Spectroelectrochemistry, J. Am. Chem. Soc. 135 (2013) 12818–12826.

[60] M.D. Levi, S. Sigalov, D. Aurbach, L. Daikhin, In Situ Electrochemical Quartz Crystal Admittance Methodology for Tracking Compositional and Mechanical Changes in Porous Carbon Electrodes, J. Phys. Chem. C. 117 (2013) 14876–14889.

[61] F. Kaasik, T. Tamm, M.M. Hantel, E. Perre, A. Aabloo, E. Lust, et al., Anisometric charge dependent swelling of porous carbon in an ionic liquid, Electrochem. Commun. 34 (2013) 196–199.

[62] J. Torop, M. Arulepp, T. Sugino, K. Asaka, A. Jänes, E. Lust, et al., Microporous and Mesoporous Carbide-Derived Carbons for Strain Modification of Electromechanical Actuators, Langmuir. 30 (2014) 2583–2587.

[63] D.M. Kolb, UV-visible reflectance spectroscopy, in: Spectroelectrochemistry, Springer, 1988: pp. 87–188.

[64] F. Rana, Graphene terahertz plasmon oscillators, Nanotechnol. IEEE Trans. On. 7 (2008) 91–99.

[65] L. Ju, B. Geng, J. Horng, C. Girit, M. Martin, Z. Hao, et al., Graphene plasmonics for tunable terahertz metamaterials, Nat Nano. 6 (2011) 630–634.

[66] Y. Li, H. Yan, D.B. Farmer, X. Meng, W. Zhu, R.M. Osgood, et al., Graphene plasmon enhanced vibrational sensing of surface-adsorbed layers, Nano Lett. 14 (2014) 1573–1577.

[67] A.N. Grigorenko, M. Polini, K.S. Novoselov, Graphene plasmonics, Nat. Photonics. 6 (2012) 749–758.

[68] J.-H. Zhong, J.-Y. Liu, Q. Li, M.-G. Li, Z.-C. Zeng, S. Hu, et al., Interfacial capacitance of graphene: Correlated differential capacitance and in situ electrochemical Raman spectroscopy study, Electrochimica Acta. 110 (2013) 754–761.

[69] A.A. Kornyshev, N.B. Luque, W. Schmickler, Differential capacitance of ionic liquid interface with graphite: the story of two double layers, J. Solid State Electrochem. 18 (2014) 1345–1349.

[70] B. Partoens, F.M. Peeters, From graphene to graphite: Electronic structure around the K point, Phys. Rev. B. 74 (2006) 075404.

[71] G.H. Lane, Electrochemical reduction mechanisms and stabilities of some cation types used in ionic liquids and other organic salts, Electrochimica Acta. 83 (2012) 513–528.

[72] D.R. Lide, CRC handbook of chemistry and physics, CRC press, 2004.

[73] Q. Zhang, S. D'Astorg, P. Xiao, X. Zhang, L. Lu, Carbon-coated fluorinated graphite for high energy and high power densities primary lithium batteries, J. Power Sources. 195 (2010) 2914–2917.

[74] V. Gupta, T. Nakajima, Y. Ohzawa, B. Žemva, A study on the formation mechanism of graphite fluorides by Raman spectroscopy, J. Fluor. Chem. 120 (2003) 143–150.

[75] V. Suryanarayanan, S. Yoshihara, T. Shirakashi, Electrochemical behavior of carbon electrodes in organic liquid electrolytes containing tetrafluoroborate and hexafluorophosphate anionic species in different non-aqueous solvent systems, Electrochimica Acta. 51 (2005) 991–999.

[76] L. Xiao, K.E. Johnson, Electrochemistry of 1-butyl-3-methyl-1H-imidazolium tetrafluoroborate ionic liquid, J. Electrochem. Soc. 150 (2003) E307–E311.

[77] J.K. Foley, C. Korzeniewski, S. Pons, Anodic and cathodic reactions in acetonitrile/tetra-n-butylammonium tetrafluoroborate: an electrochemical and infrared spectroelectrochemical study, Can. J. Chem. 66 (1988) 201–206.

[78] V. Dinoiu, Chemical Fluorination of Organic Compounds, Rev. Roum. Chim. 52 (2007) 219–234.

[79] C. Tian, W. Nie, M.V. Borzov, P. Su, High-Yield Thermolytic Conversion of Imidazolium Salts into Arduengo Carbene Adducts with BF3 and PF5, Organometallics. 31 (2012) 1751–1760.

8. Figures

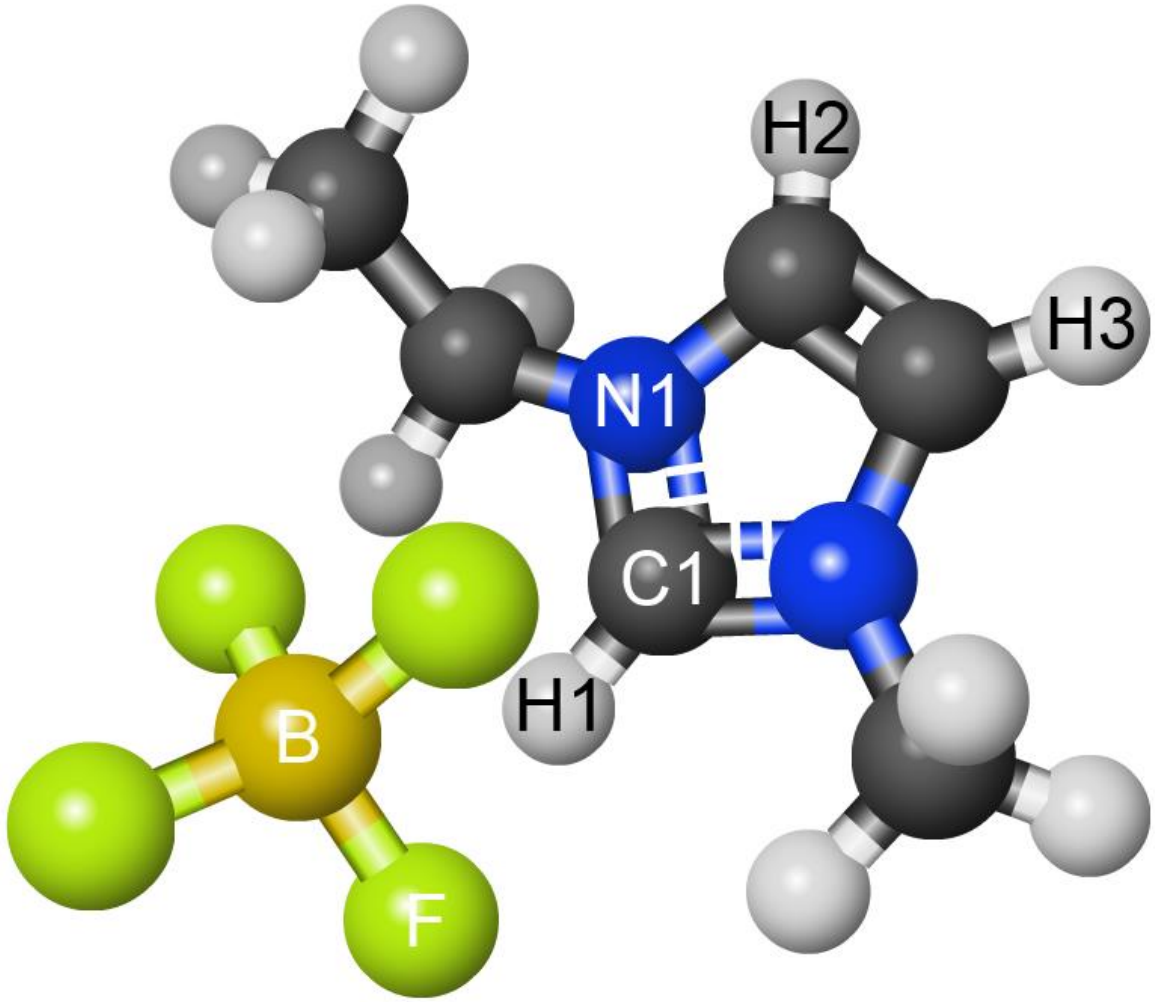

Figure 1: Optimized ionic pair structure with atom notations used trough the thesis.

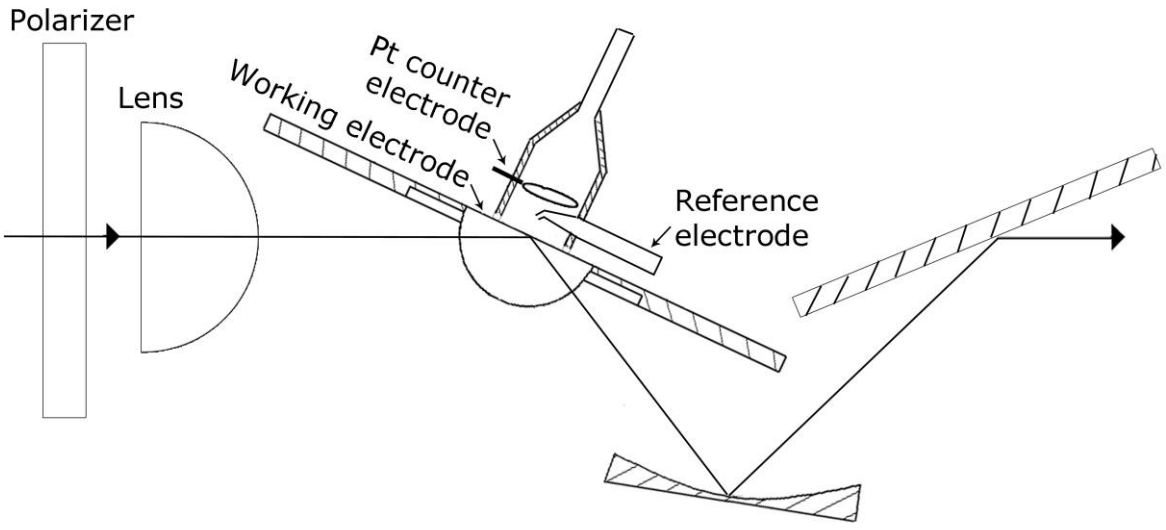

Figure 2: General measurement scheme for *in situ* infrared spectroelectrochemistry.

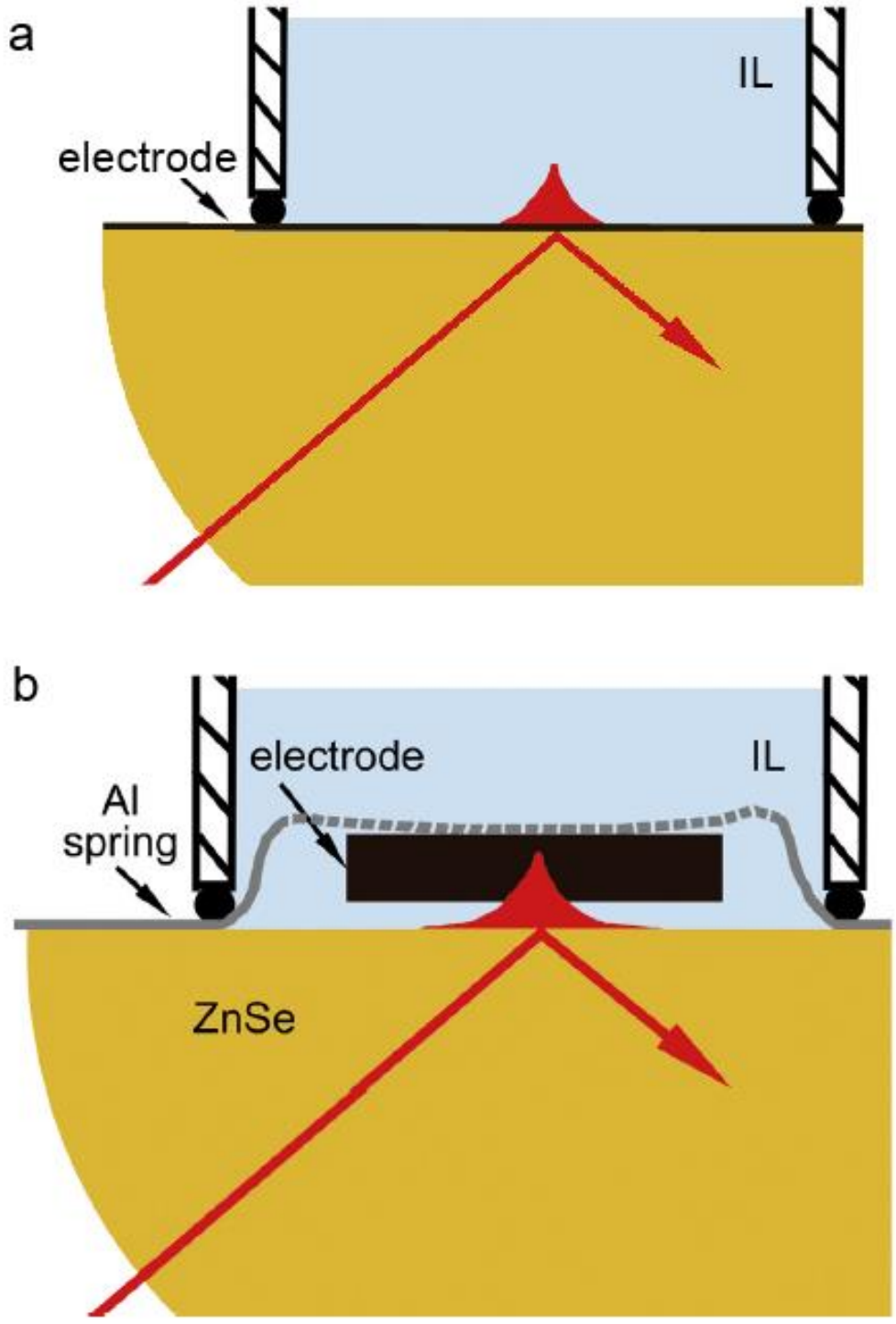

Figure 3: Measurement scheme for *in situ* infrared absorption spectroscopy (IRAS) (a) and infrared reflection-absorption spectroscopy (IRRAS) (b) measurements.

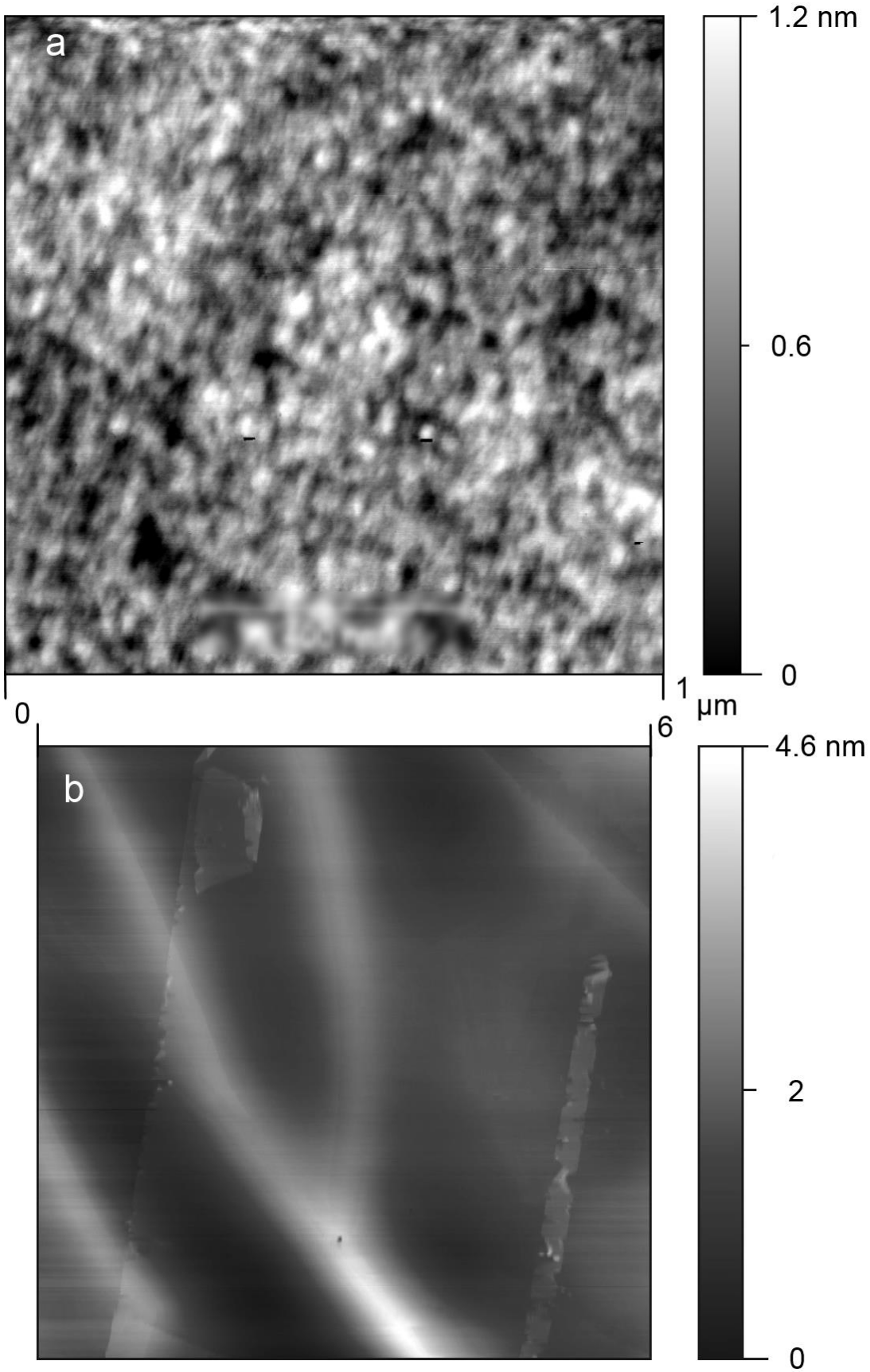

Figure 4: AFM topography images of (a) 20 nm amorphous carbon (aC) and (b) few-layer graphene electrodes (FLG).

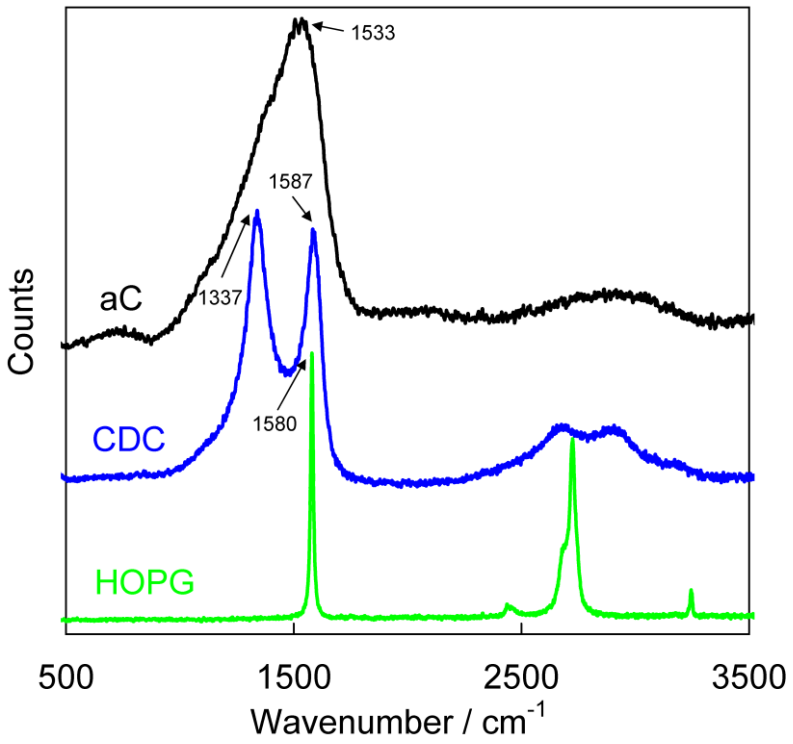

Figure 5: Raman spectra of the different carbon electrodes used in the thesis.

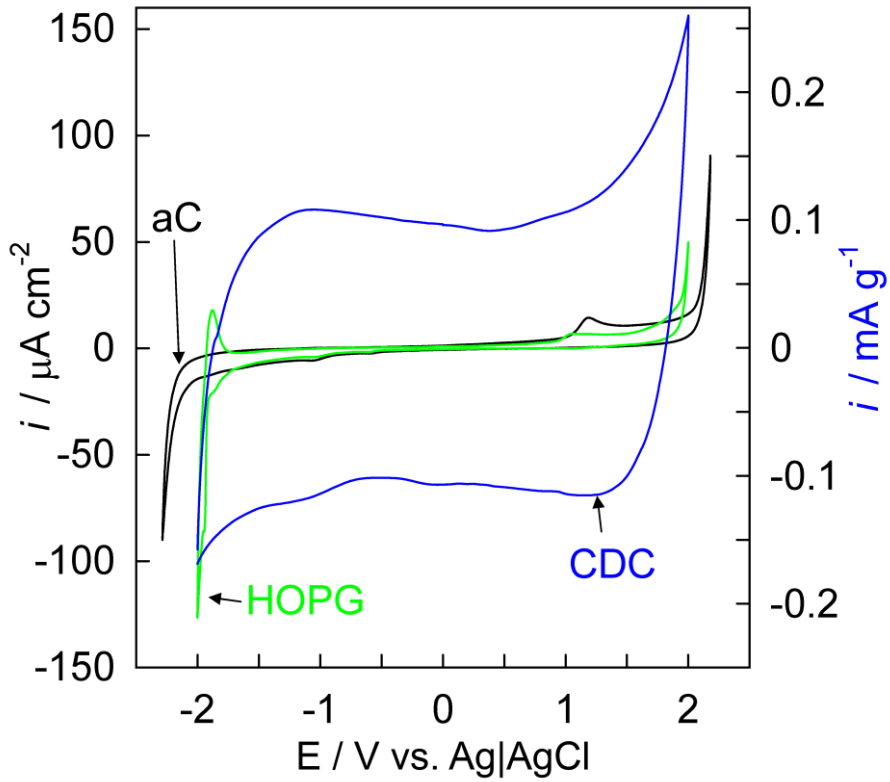

Figure 6: Cyclic voltammograms (CV) at potential scan rate of 10 mV s^{-1} (HOPG and aC) and 1 mV s^{-1} (CDC) of the three different carbon electrodes used in the thesis measured in $EMImBF_4$.

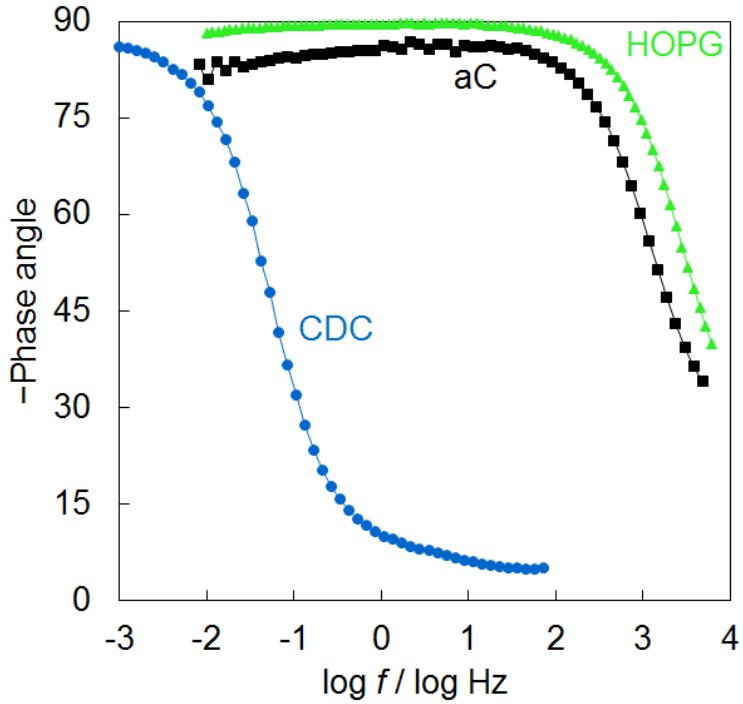

Figure 7: Electrochemical impedance spectroscopy phase angle diagrams of the three different carbon electrodes used in the thesis measured at the pzc in $EMImBF_4$.

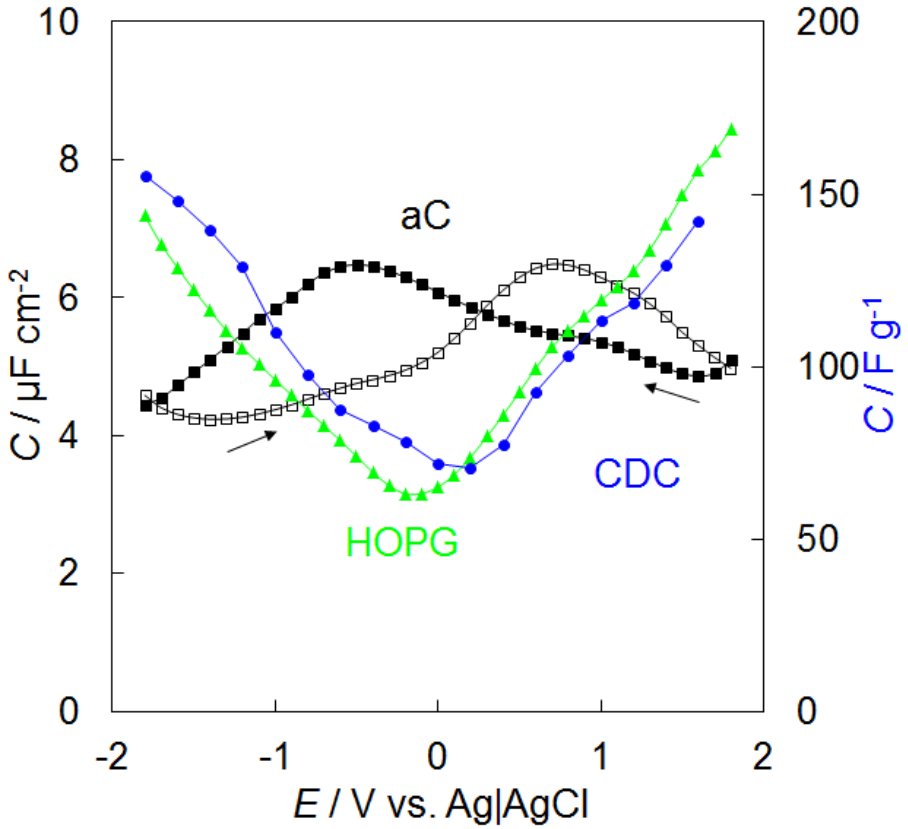

Figure 8: Differential capacitance- potential (CE) graphs at 200 Hz (HOPG and aC) and 1 mHz (CDC) of the three different carbon electrodes used in the thesis measured in $EMImBF_4$.

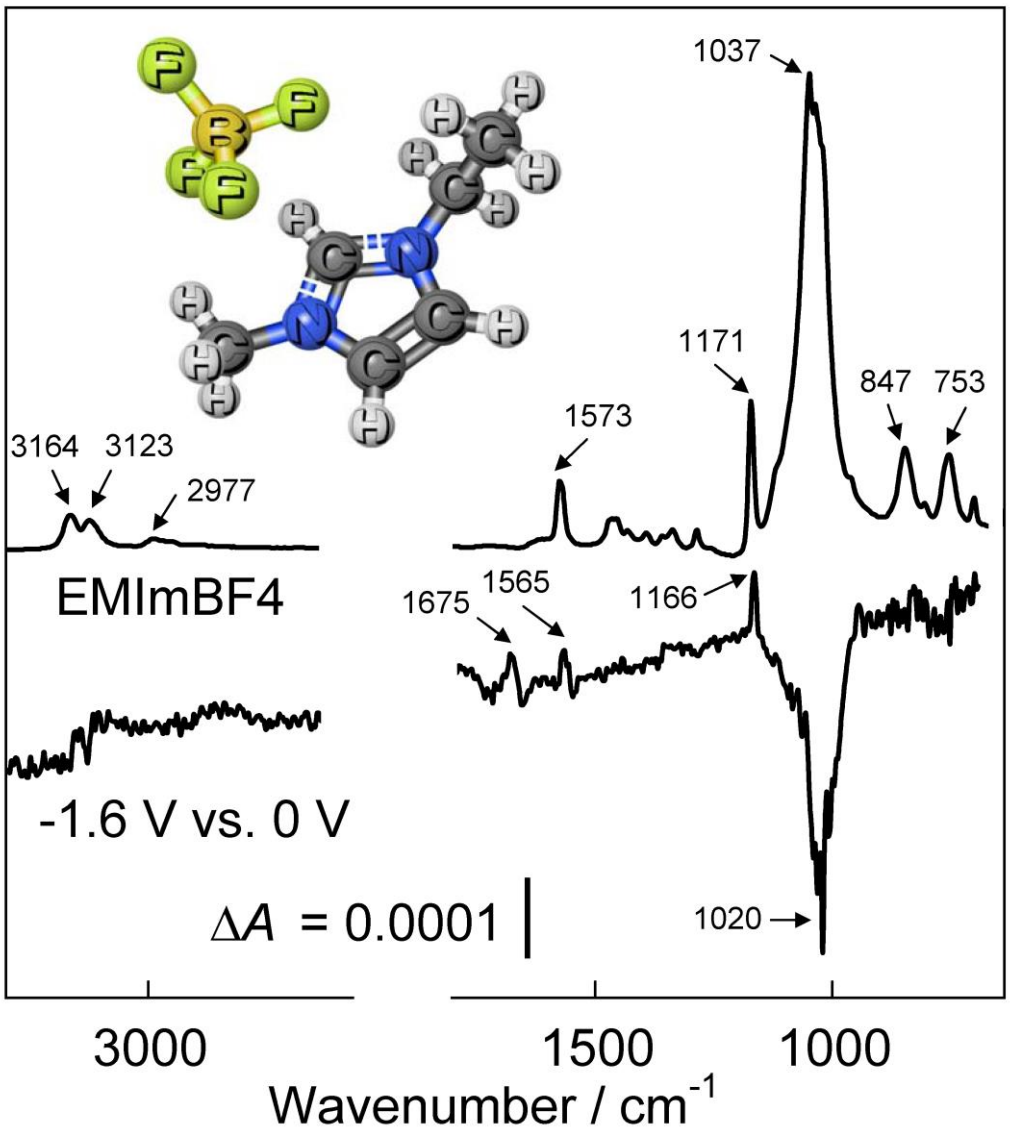

Figure 9: Comparison of the ATR spectrum of $EMImBF_4$ calculated for monolayer adsorption with the p-polarized *in situ* IRAS spectra of the 20 nm aC | $EMImBF_4$ interface measured at −1.6 V relative to the reference potential at 0 V.

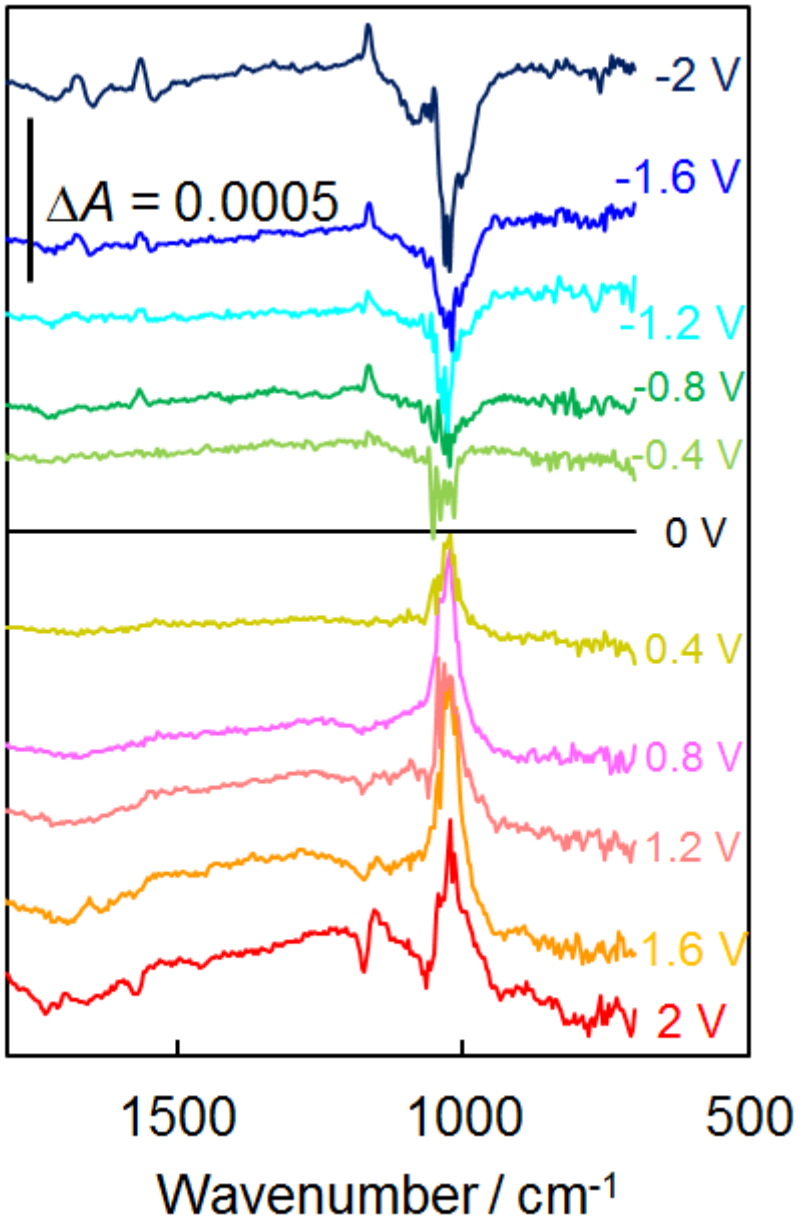

Figure 10: P- polarized *in situ* IRAS spectra of the 20 nm aC | $EMImBF_4$ interface measured relative to the reference spectrum at 0 V. The spectra are shifted by a constant in the vertical direction for clarity.

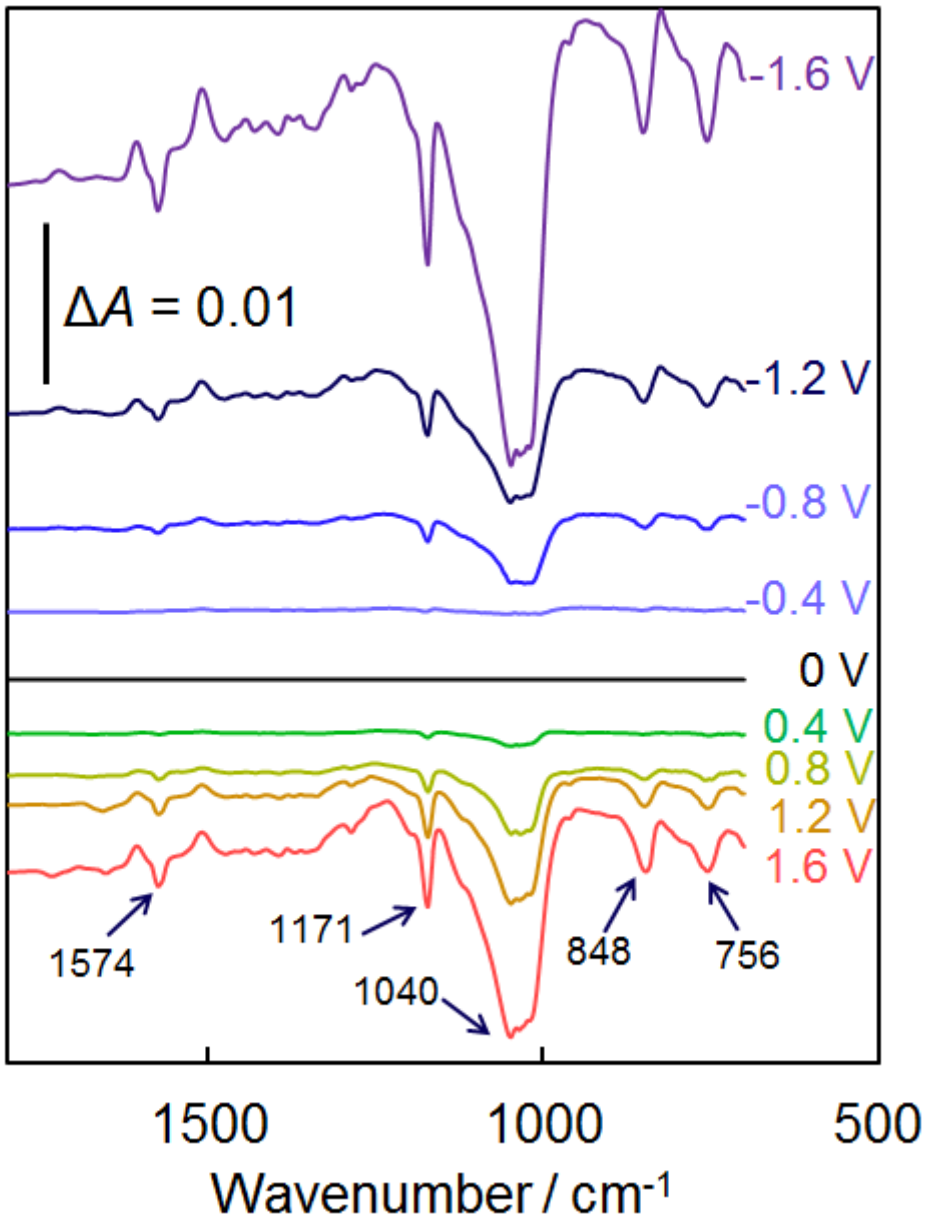

Figure 11: P- polarized *in situ* IRRAS spectra of the CDC(TiC) | $EMImBF_4$ interface measured relative to the reference spectrum at 0 V. The spectra are shifted by a constant in the vertical direction for clarity.

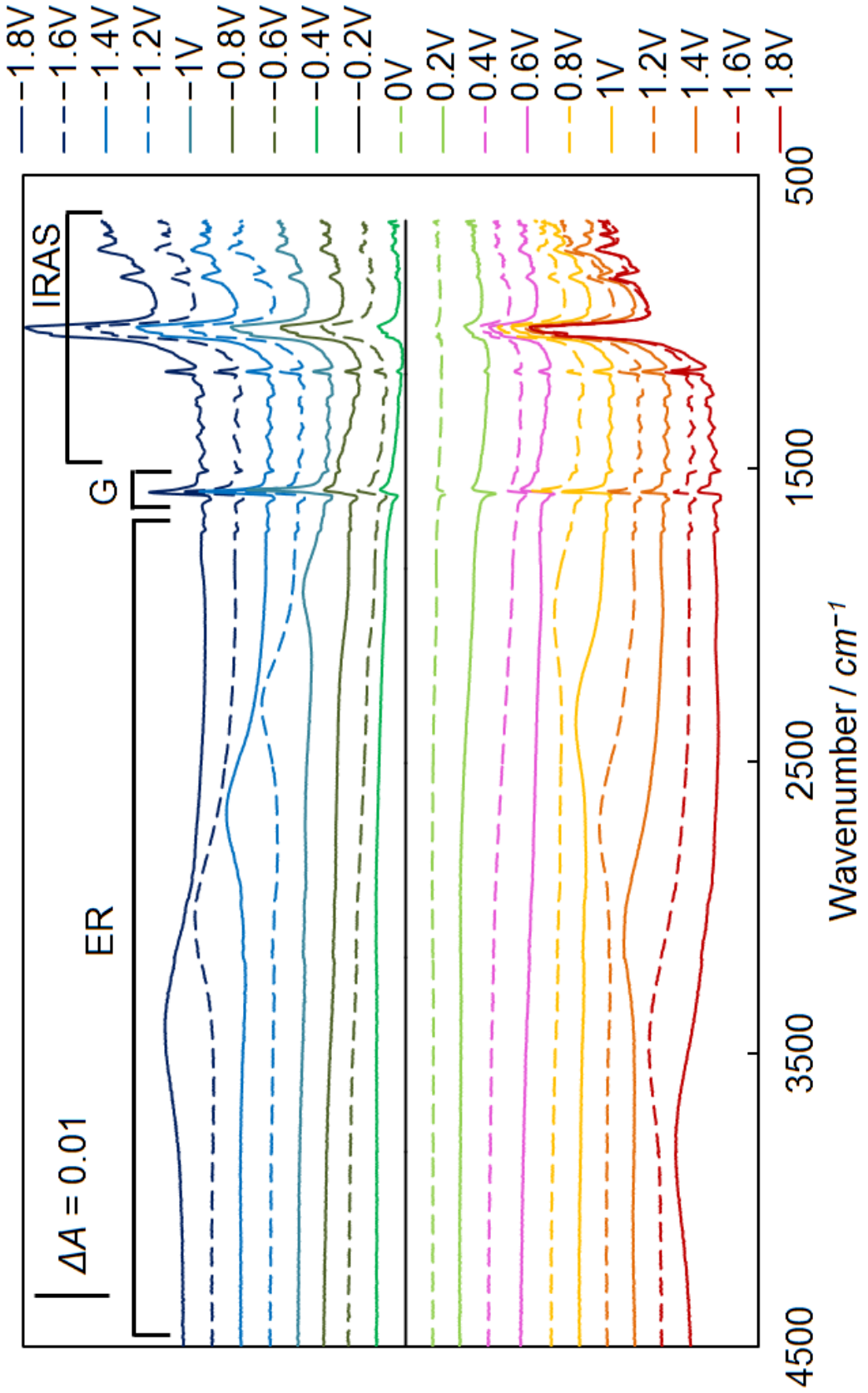

Figure 12: P-polarized *in situ* infrared spectra of the FLG|EMImBF$_4$ interface measured relative to the reference spectrum at pzc. The spectra are shifted in the vertical direction for clarity. Areas where different spectral information has been extracted have been outlined.

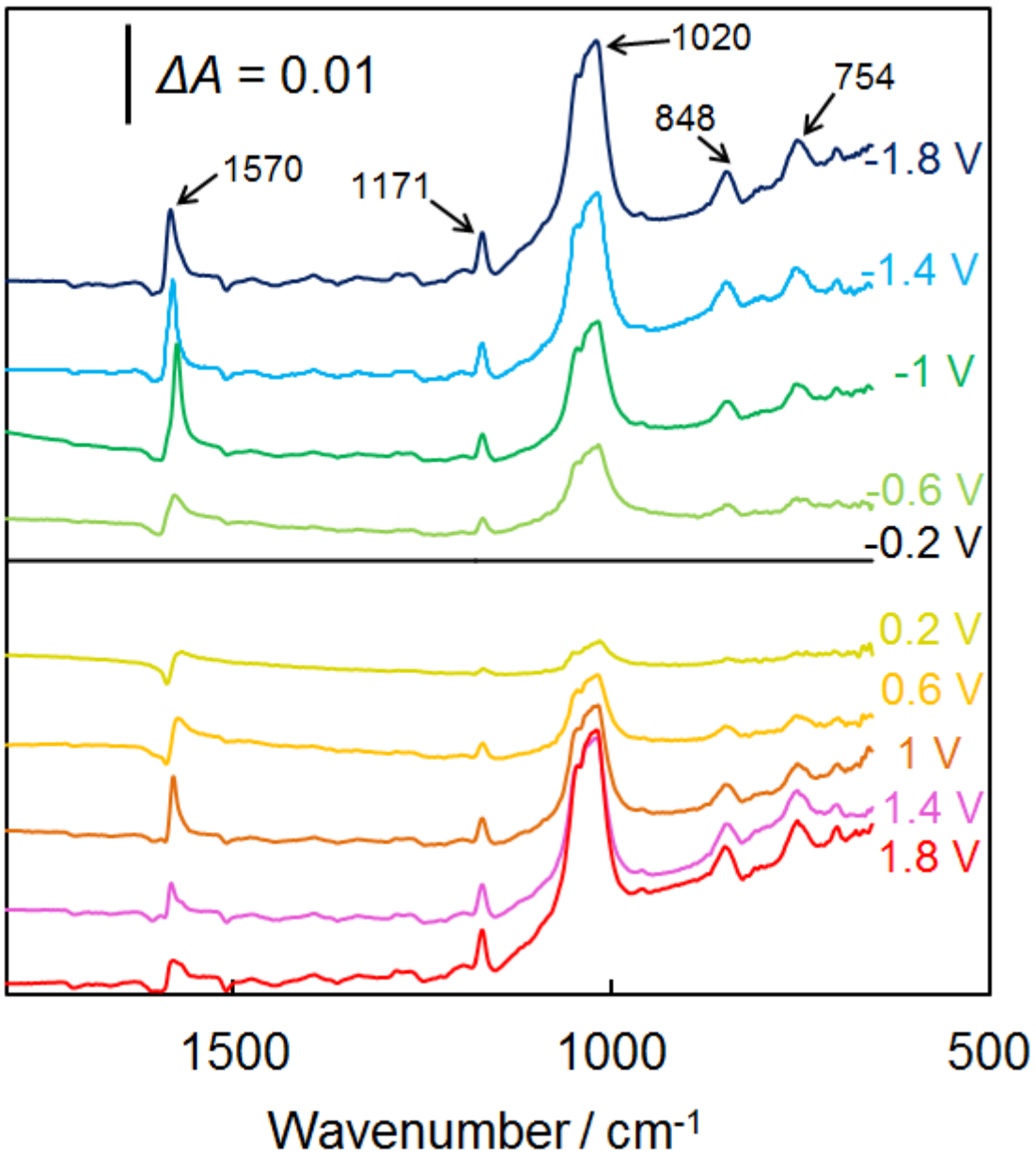

Figure 13: P- polarized *in situ* IRAS spectra of the FLG|EMImBF$_4$ interface measured relative to the reference spectrum at pzc. The spectra are shifted by a constant in the vertical direction for clarity.

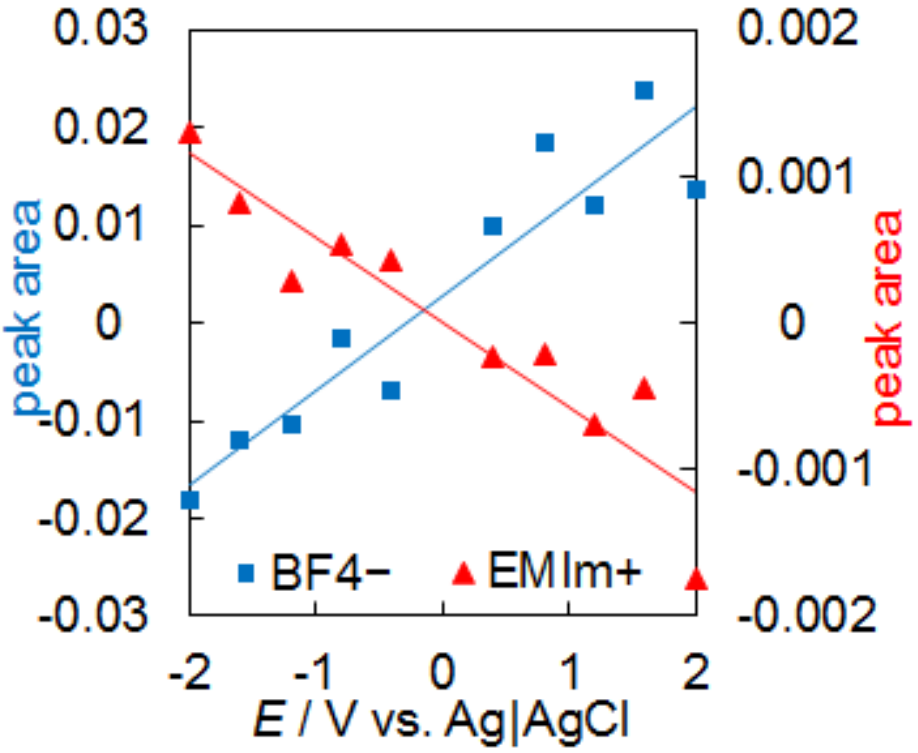

Figure 14: Comparison of the (■) anion and (▲) cation peak areas relative to the applied potential for the *in situ* IRAS spectra of the 20 nm aC | $EMImBF_4$ interface measured relative to the reference spectrum at 0 V from the data seen in Figure 10.

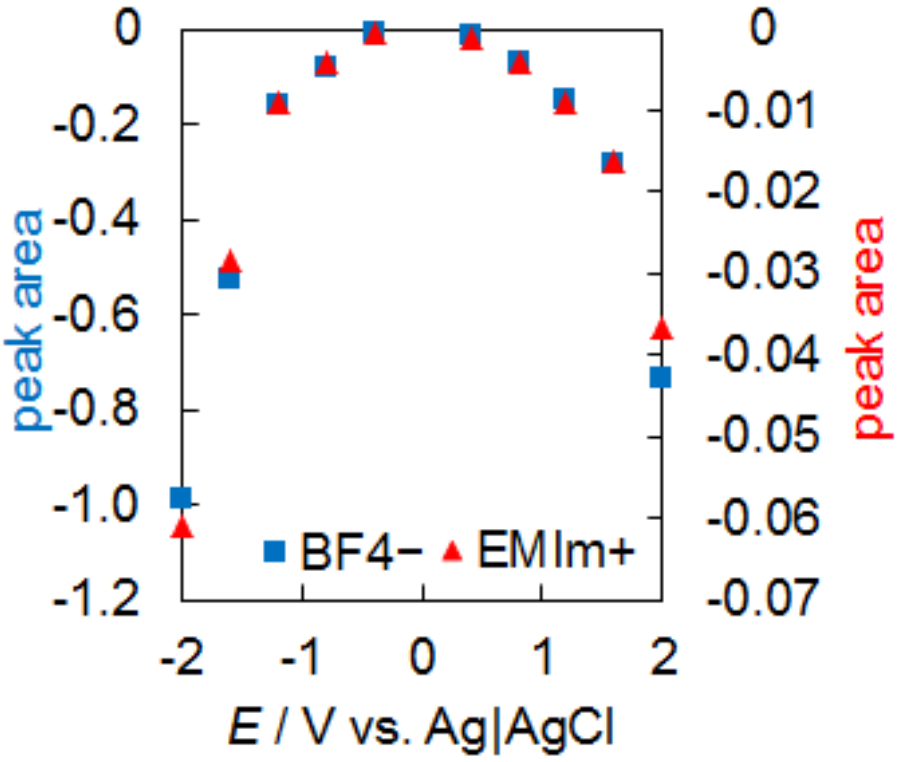

Figure 15: Comparison of the (■) anion and (▲) cation peak areas relative to the applied potential for the *in situ* IRRAS spectra of the CDC(TiC) | $EMImBF_4$ interface measured relative to the reference spectrum at 0 V from the data seen in Figure 11.

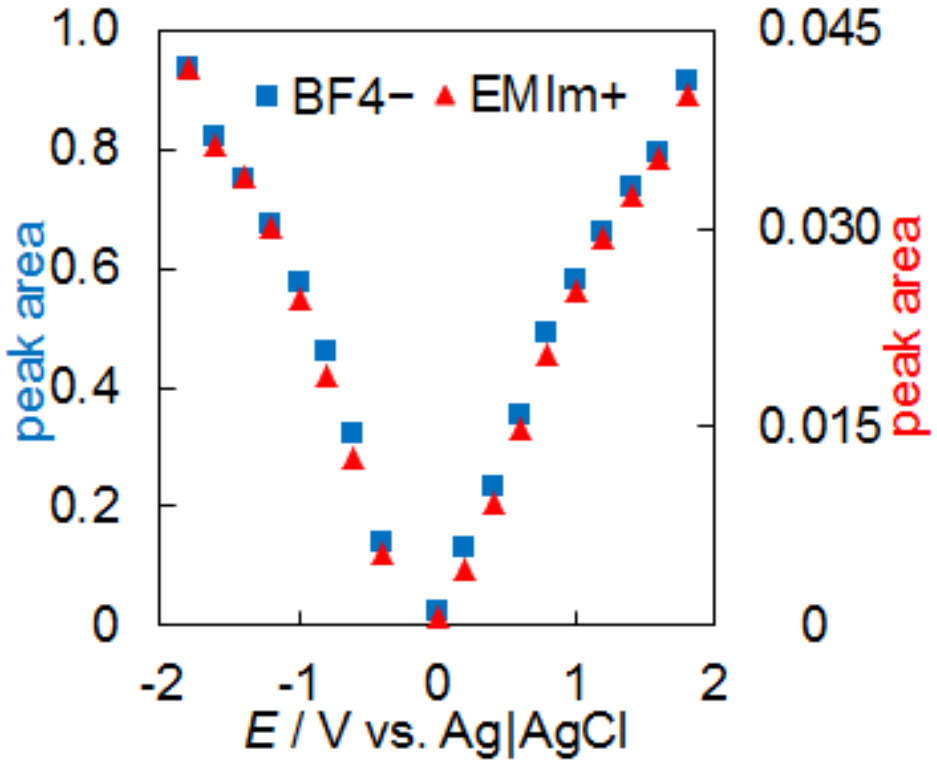

Figure 16: Comparison of the (■) anion and (▲) cation peak areas relative to the applied potential for the *in situ* IRAS spectra of the FLG|EMImBF_4 interface measured relative to the reference spectrum at the pzc from the data seen in Figure 12.

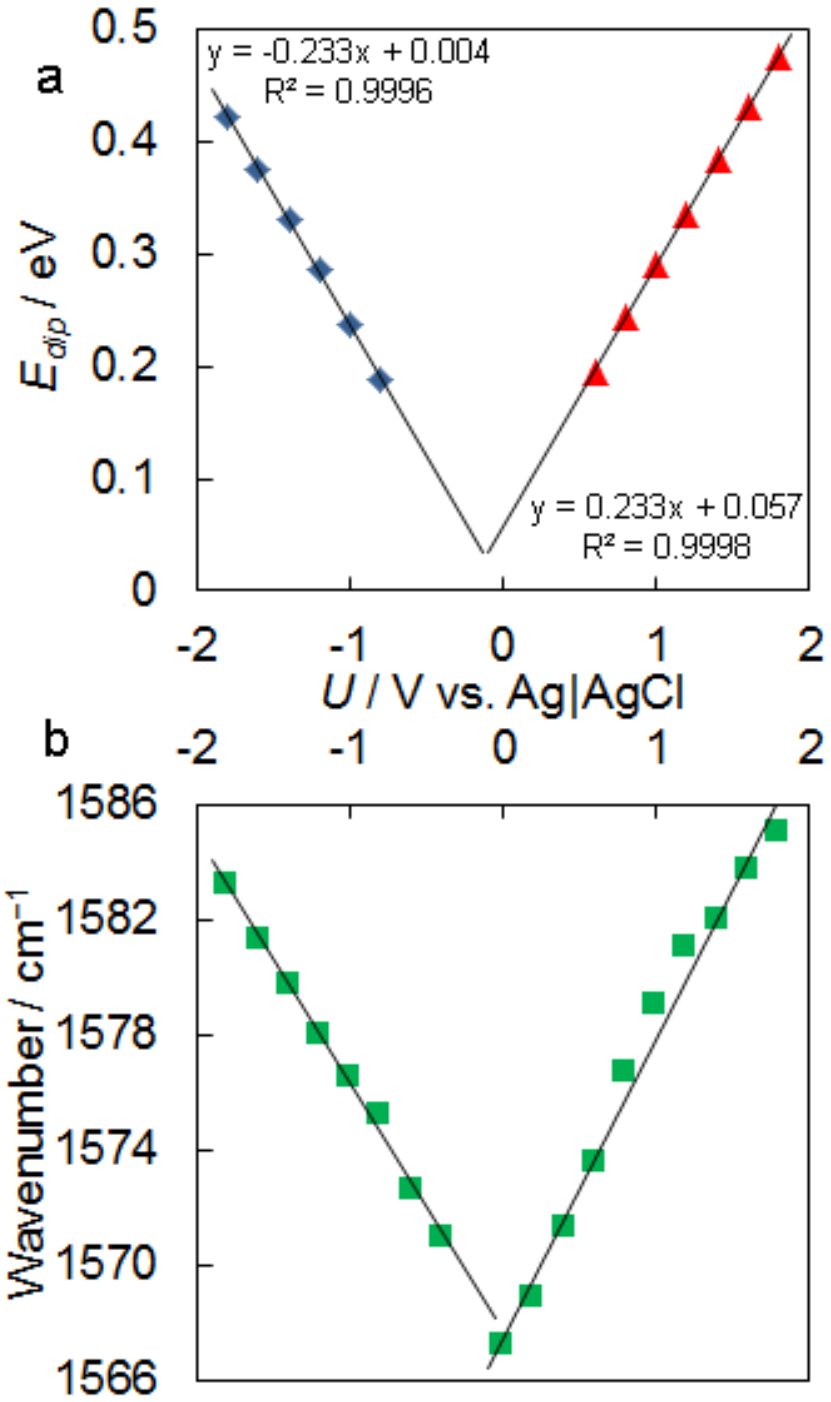

Figure 17: The dependences of Edip (a) and G band position (b) on electrode potential from the data seen in Figure 12.

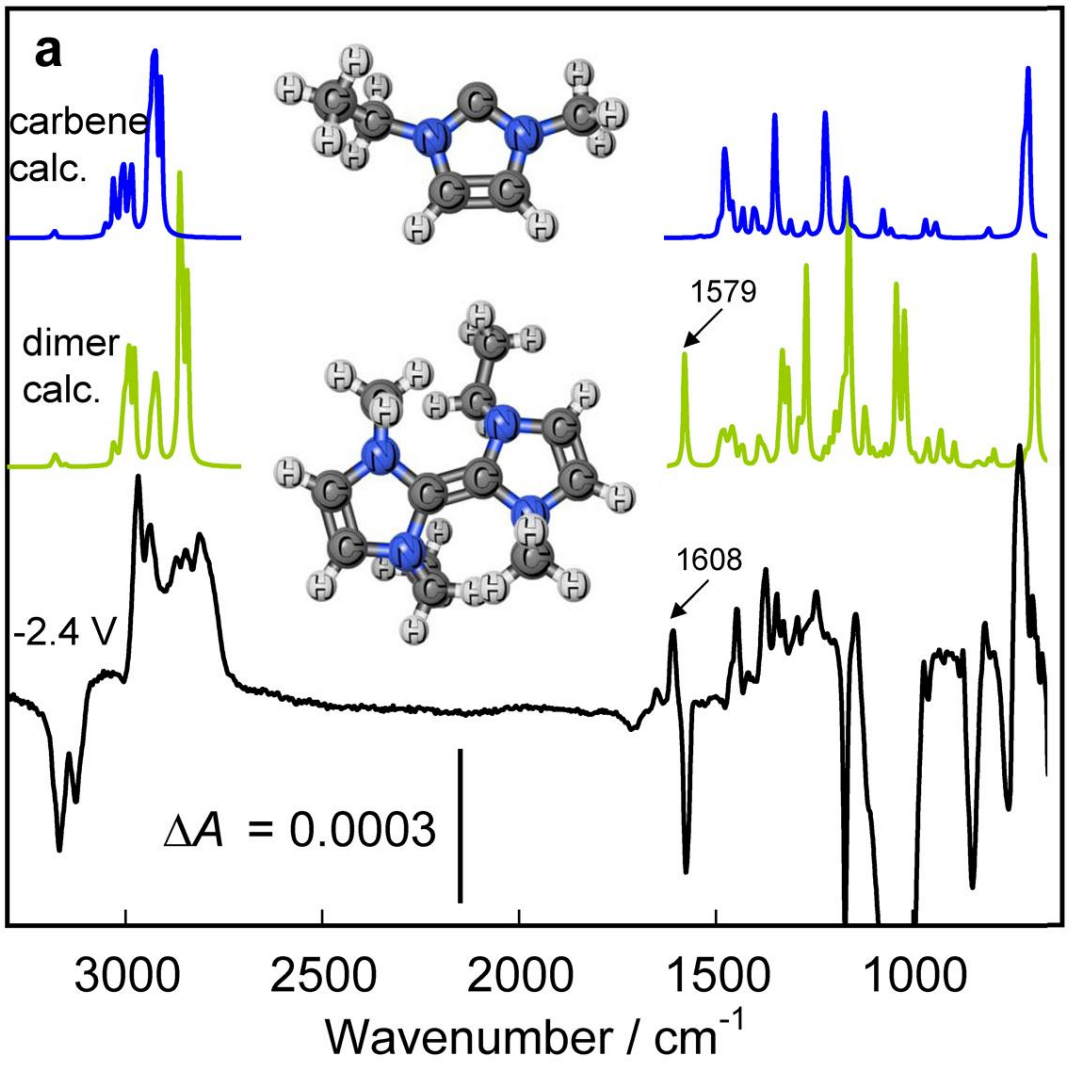

b

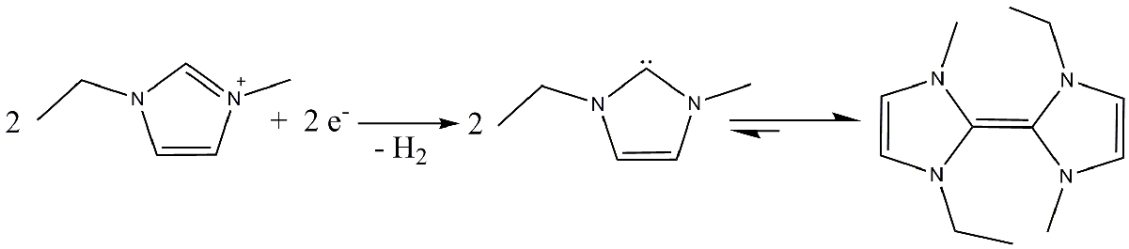

Figure 18: Experimentally measured and calculated spectra of the reaction products at −2.4 V (a) and the reaction scheme (b).

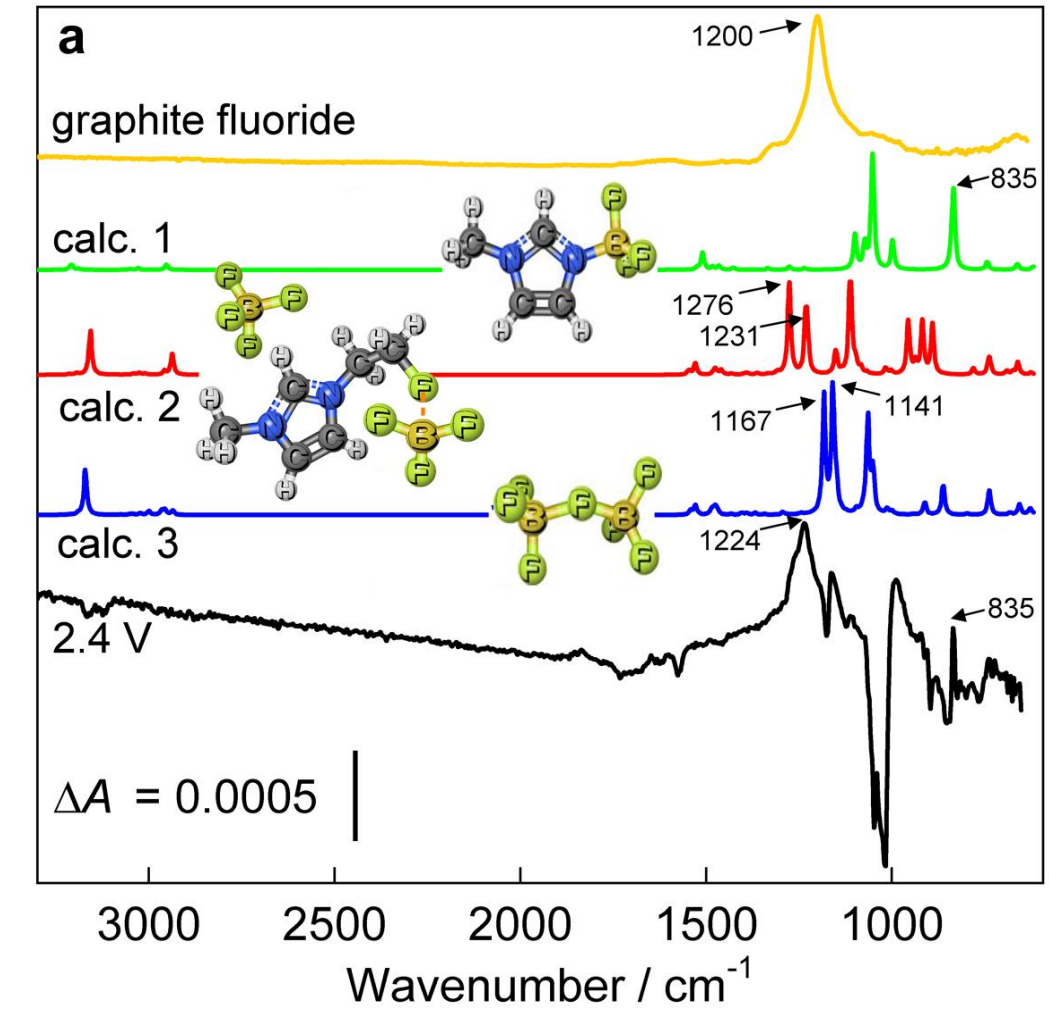

b

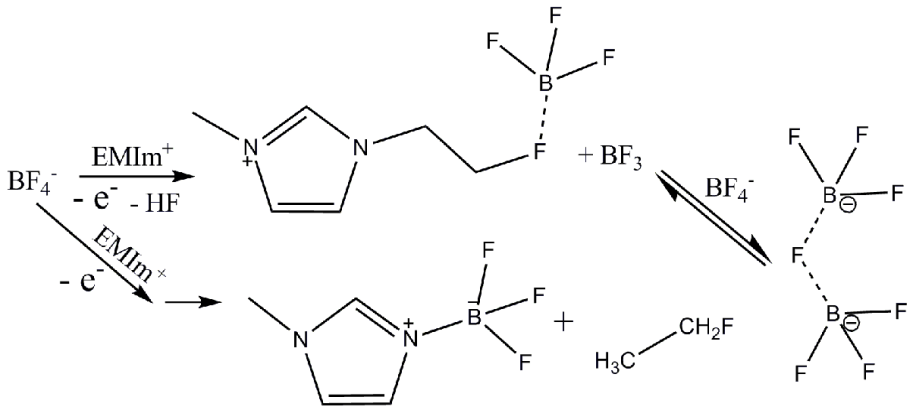

Figure 19: Experimentally measured and calculated spectra of the reaction products at $E > 2$ V (a) and proposed reaction scheme (b).

9. Publications

1. T. Romann, O. Oll, P. Pikma, H. Tamme, E. Lust, Surface chemistry of carbon electrodes in 1-ethyl-3-methylimidazolium tetrafluoroborate ionic liquid – an *in situ* infrared study, Electrochimica Acta, 125 (2014) 183.

2. O. Oll, T. Romann, E. Lust, An infrared study of the few-layer graphene | ionic liquid interface: reintroduction of *in situ* electroreflectance spectroscopy, Electrochemistry Communications, Accepted.

Non-exclusive licence to reproduce thesis and make thesis public

I, Ove Oll,

1. herewith grant the University of Tartu a free permit (non-exclusive licence) to:

1.1. reproduce, for the purpose of preservation and making available to the public, including for addition to the DSpace digital archives until expiry of the term of validity of the copyright, and

1.2. make available to the public via the university's web environment, including via the DSpace digital archives, as of **01.06.15** until expiry of the term of validity of the copyright,

In situ INFRARED SPECTROELECTROCHEMICAL MEASUREMENTS OF CARBON ELECTRODES IN IONIC LIQUID MEDIUM,

supervised by Tavo Romann,

2. I am aware of the fact that the author retains these rights.

3. This is to certify that granting the non-exclusive licence does not infringe the intellectual property rights or rights arising from the Personal Data Protection Act.

Tartu, **27.05.14**